Robotica (2016) volume 34, pp. 1437–1463. © Cambridge University Press 2014
doi:10.1017/S0263574714002379

A new observer-based adaptive controller for cooperative handling of an unknown object

Reza Monfaredi†‡*, S. Mehdi Rezaei† and Ali Talebi§

†*Mechanical Engineering Department and New Technology Research Center, University of Amirkabir, Tehran, Iran*
‡*Children's National Medical Center, Washington DC, USA*
§*Electrical Engineering Department and New Technology Research Center, University of Amirkabir, Tehran, Iran*

(Accepted August 12, 2014. First published online: September 12, 2014)

SUMMARY
This paper presents a new observer-based adaptive controller for handling an object with *unknown* geometry, center of mass, and inertia using a cooperative robotic system. The cooperative robotic system comprises three Cartesian robots, where robots and the grasped object form a closed-loop kinematic chain. The unknown object is approximated by three virtual links of unknown lengths rigidly attached to one another at the object's center of mass (COM). Due to the unknown COM and unknown inertia of the object, the lengths and inertia of these virtual links are unknown, resulting in kinematic and dynamic uncertainties in the control system. A parameter estimator is proposed to estimate the object's COM to compensate for kinematic uncertainties of the system. Moreover, a new dynamic adaptation law is developed to cope with dynamic uncertainties of the object. The dynamic equations of the cooperative system are transformed from joint space into task space. These task space dynamics are transformed into object space by passively decomposing the dynamics into two decoupled systems, i.e. *locked* and *shaped* systems. An adaptive controller is developed for the locked system, and the shaped system is controlled by a composite controller based on a PD controller plus a stabilizing damping term. The stability of the proposed controllers is shown using the passivity concept and Lyapunov theorem. Simulation results show that the closed-loop position error asymptotically converges to zero. It is also shown that kinematic and dynamic adaptation parameters converge to real and bounded values respectively.

KEYWORDS: Cooperative robotic system; Unknown object; Dynamic uncertainty; Kinematic uncertainty; Observer-based adaptive control.

1. Introduction

Cooperative robotic arms that work together in the presence of kinematic and dynamic uncertainty of the environment could mimic the dexterity and performance of human arms in handling objects to a large extent. A cooperative robotic system could be used to manipulate a wide range of objects with different shapes and geometries. It avoids the use of customized grippers for different objects, thus being useful in industrial and space applications. A cooperative robotic system has other advantages over a single-robot system, such as improved handling capability and increased loading capacity.

Although a significant amount of research in coordinated adaptive control of robot manipulators with dynamic uncertainties has been investigated,[1–3] adaptive control of a robotic system with kinematic uncertainty has not been widely investigated. Studies that consider kinematic uncertainty are limited to the set point control problem.[4,5] Cheah *et al.* developed trajectory tracking control of a robotic system with kinematic uncertainty.[6,7] This approach has been developed for controlling a *single* robotic manipulator with kinematic and dynamic uncertainties (e.g. unknown length and weight/inertia of the links respectively). The uncertainty originated from an unknown external link

* Corresponding author. E-mail: rmonfare@cnmc.org

https://doi.org/10.1017/S0263574714002379 Published online by Cambridge University Press

(object) that was connected to the end of the manipulator. The object's tip position was measured using a transitional position sensor in the task space. This approach cannot be extended to cooperative systems because the center of mass (COM) for a geometrically unknown object is unknown and cannot be measured using a transitional position sensor.

Some studies have considered handling of an object with known COM.[8–10] Cooperative handling of an object via three robots has been investigated by Lee *et al.*, in which an object with known shape was considered.[11,12] Sirouspour developed a multi-master multi-slave (MMMS) cooperative telerobotic system in which the slave robots cooperatively manipulate a known tool to perform a task on an environment.[13] A decentralized, adaptive, coordinated control method without a force sensor was proposed in Kawasaki *et al.*[14] for multiple robot arms grasping a common object. Cases of rigid contact and rolling contact between robots and the object were analyzed. However, it was assumed that the object's COM is measurable. Tang and Krovi focused on the development of a quantitative performance analysis framework for a cooperative system of multiple wheeled mobile manipulators transporting a common object.[15] However, the common object was assumed to have a known triangular geometry. Sarikaya *et al.* developed an adaptive and robust controller for handling a known object with known COM by cooperative manipulation using two three-dimensional revolute-jointed manipulators.[16] A virtual linkage model was developed to determine the inner forces using the multiple impedance control law when an object with known COM was handled by a cooperative robotic system.[17] A cooperative robotic system with under-actuated manipulators was developed to handle an object with known COM, using a hybrid force/position controller.[18] A new approach has been developed for handling an object of unknown geometry, based on the estimation of COM.[19] Three 3-degree of freedom (DOF) force sensors were required to estimate center of gravity of the object using a novel algorithm. Proportional-derivative (PD) and proportional-integral-derivative (PID) controllers were employed for *shaped* and *locked* systems respectively. This control algorithm is limited to 3-DOF transitional motion.

A novel approach was proposed in ref. [20], which provided transitional as well as rotational movement of the object without using a force sensor. Two basic PD controllers were used for the shaped and locked systems. A robust adaptive[21] and adaptive hybrid controller[22,23] were developed for the handling of a planar unknown object using two planar manipulators where the COM is assumed to be in the center of the object.

To the best of the authors' knowledge, there is a lack of research in the field of controlling of a cooperative robotic system for handling an unknown object. Spatial handling of an unknown object with both kinematic uncertainty (unknown geometry and COM) and dynamic uncertainty has not been addressed in the literature.

In this study, a new approach is proposed to control a cooperative robotic system for translational and rotational handling of an unknown object in 6-DOF. Both kinematic and dynamic uncertainty is considered, and a model-based controller is developed for a cooperative robotic system by incorporating an observer for COM estimation.

Table I summarizes the previous studies in the field of cooperative robotic systems and compares them against the current study.

In the current study, it is assumed that the three-dimensional object has unknown geometry, COM, and inertia. It is assumed that mass of the object is known for the control system. Since three force sensors are used at the contact points for the proposed approach, for experimental implementation the weight of the object can be easily measured by reading the force sensors and using the kinematics of robots to calculate the force component in the direction of the gravity. Therefore, the measured mass of the object could be available for the control system. However, the inertia of the object is assumed to be unknown. Therefore, in the proposed control system, a dynamic adaptation law and a parameter estimator are proposed to compensate both dynamic and kinematic uncertainties respectively.

The locked system is controlled by an adaptive controller and the shaped system is controlled by a composite controller. The composite controller, based on a PD controller and a damping term to stabilize the shaped system, incorporates the effect of estimated kinematic parameters in the control law.

The unknown object is modeled as three virtual links. A virtual link is an imaginary link that connects the contact point between a robot and the object to the object's COM. It is possible to find three virtual links that are rigidly connected to each other at the COM and have equivalent mass,

https://doi.org/10.1017/S0263574714002379 Published online by Cambridge University Press

Table I. Comparison of prior studies with the current study.

References	Unknown object		Cooperative system	Spatial motion (6-DOF)	Others
	Unknown geometry	Unknown dynamics			
Cheah *et al.*[4–7]			×		-
Gudiño-Lau *et al.*[8,9]	×	×		×	-
Tsuji *et al.*[10]	×	×			-
Lee *et al.*[11,12]	×	×		×	-
Sirouspour *et al.*[13]	×	×		×	-
Kawasaki *et al.*[14]	×				-
Tang *et al.*[15]	×	×		×	-
Sarikaya *et al.*[16]	×				-
Rastegari *et al.*[17]	×	×			-
Tinós *et al.*[18]	×	×		×	-
Monfaredi *et al.*[19]				×	Non-model-based controller
R. Monfaredi *et al.*[20]					Non-model-based controller
Mohajerpoor *et al.*[21–23]	×			×	-
Current paper					Model-based adaptive controller and stability analysis

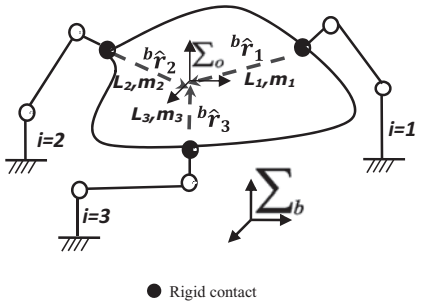


Fig. 1. Object is modeled by three virtual links as shown above with dashed vectors.

inertia, and COM compared with the original object. Virtual links are shown in Fig. 1 using three broken lines.

In Fig. 1, Σ_b is the base frame (i.e. the reference frame for all other frames). Σ_o is the object frame, which is located in the COM and has the same orientation as the base frame. Σ_o' is the frame attached to COM, which rotates with the object.

2. Modeling of Cooperative System

The cooperative system considered in this paper consists of three 6-DOF robots, each of which is extended by a virtual link. Therefore, the cooperative system is considered as a set of three extended robots (robot plus virtual link) that are connected to each other at the COM. Virtual links are connected to each other in the estimated COM and form a closed-loop kinematic chain as shown in Fig. 1.

Assumptions for the current study are as follows:

1. The Object has unknown geometry, COM, and inertia.
2. The Object has known mass.
3. Three contacts between object and robots are rigid, hence no rotation or slippage is allowed at the contact points.
4. The Object is rigid and COM is not changing.
5. It is assumed that proper contact points are given.

https://doi.org/10.1017/S0263574714002379 Published online by Cambridge University Press

In this section, the dynamic equation of the cooperative robotic system is derived by two sequential transformations. First, the joint space dynamic equations of the system are transformed into the task space using Jacobian metrics. In the next step, the task space dynamic equations are transformed into the object space (i.e. shaped and locked systems) using the decomposition matrix. The joint space, task space, and object space equations of the cooperative robotic system are given in the following sections respectively.

2.1. Joint space coordinate system

The dynamic equation of each robot with respect to a common inertial frame is given by the following equation[11]:

$$\mathbf{M_i}\left(\boldsymbol{q_i}\right)\ddot{\boldsymbol{q}}_i + \mathbf{C_i}\left(\boldsymbol{q_i}, \dot{\boldsymbol{q}}_\iota\right)\dot{\boldsymbol{q}}_i = \boldsymbol{\tau}_i + \mathbf{J_i^T}(\boldsymbol{q_i})\boldsymbol{F}_i,\ i = \{1, 2, 3\}, \tag{1}$$

where $\boldsymbol{q_i} = [q_{i1}\, q_{i2}\, q_{i3}\, q_{i4}\, q_{i5}\, q_{i6}]^{\mathrm{T}}$ is the generalized coordinate vector of each robot, $\mathbf{M}_{\mathrm{i}}(\boldsymbol{q_i})\varepsilon\mathrm{R}^{6\times6}$ is the positive definite inertia matrix of the *i*th extended robot. $\mathbf{C_i}(\boldsymbol{q_i}, \dot{\boldsymbol{q}}_\iota)$ is the Coriolis matrix. Moreover, $\boldsymbol{\tau_i} \in \mathbf{R}^6$ and $\boldsymbol{F_i} \in \mathbf{R}^6$ are the generalized force to be designed and external force respectively, and $\mathbf{J_i^T}(\mathrm{q}) \in \mathbf{R}^{6\times6}$ is the Jacobian matrix for transformation from the joint space into the task space (more details are presented in Appendix A; see Appendix B for notations).

Several important properties of dynamic Eq. (1) are given below.[3]

Property 1: The inertia matrix $\mathbf{M_i}(\boldsymbol{q_i})$ is symmetric and uniformly positive definite for all $\boldsymbol{q_i} \in \boldsymbol{R^n}$.
Property 2: The matrix $\dot{\mathbf{M}}_\mathbf{i} - 2\mathbf{C_i}$ is skew-symmetric so that $\dot{\boldsymbol{q}}_i^T(\dot{\mathbf{M}}_\mathbf{i} - 2\mathbf{C_i})\dot{\boldsymbol{q}}_\iota = 0$ for all $\boldsymbol{q_i}, \dot{\boldsymbol{q}}_\iota \in \boldsymbol{R}^6$.
Property 3: The dynamic model (1) is linear in a set of parameters $\boldsymbol{\theta_{id}} = [m_i I_{y,zi} I_{xi} 1]^{\mathrm{T}}$ as

$$\mathbf{M_i}\left(\mathbf{q_i}\right)\ddot{\mathbf{q}}_\mathbf{i} + \mathbf{C_i}\left(\mathbf{q_i}, \dot{\mathbf{q}}_\mathbf{i}\right)\dot{\mathbf{q}}_\mathbf{i} = \mathbf{Y_i}\left(\mathbf{q_i}, \dot{\mathbf{q}}_\mathbf{i}, \ddot{\mathbf{q}}_\mathbf{i}\right)\boldsymbol{\theta}_\mathbf{id}, \tag{2}$$

where $\boldsymbol{\theta_{id}}$ is the dynamic parameter vector, and $\mathbf{Y_i}(\boldsymbol{q_i}, \dot{\boldsymbol{q}}_i, \ddot{\boldsymbol{q}}_i) \in \mathbf{R}^{6\times4}$ is the so-called dynamic regressor matrix of the *i*th extended robot, m_i is the mass of the *i*th virtual link, and $I_{y/zi}$ ($I_{y/zi}$ represents both I_{yi} and I_{zi} because it is assumed that $I_{yi} = I_{zi}$ for virtual links) and I_{xi} are the moment of inertia of the *i*th virtual link with respect to the z/y and x axes respectively, where x is defined along the virtual link.

2.2. Task space dynamic equations

In order to transform the dynamic equations of the system from joint space into task space, the Jacobian matrix of the extended robot (robot plus virtual link), $\mathbf{J}_i$, is derived (see Appendix A). The Jacobian matrix of the cooperative robotic system is as follows:

$$\mathbf{J} = \begin{bmatrix} \mathbf{J}_1 & 0 & 0 \\ 0 & \mathbf{J}_2 & 0 \\ 0 & 0 & \mathbf{J}_3 \end{bmatrix}, \tag{3}$$

where $\mathbf{J}_i$ is the Jacobian matrix of the *i*th extended robot. Task space coordinate vector of the entire cooperative robotic system is defined as $\boldsymbol{X} = [\,\boldsymbol{X}_1\ \boldsymbol{X}_2\ \boldsymbol{X}_3\,]^T$. Task space coordinate vector of each extended robot is obtained as follows:

$$\dot{\boldsymbol{X}}_i = \mathbf{J_i}\left(\boldsymbol{q_i}\right)\dot{\boldsymbol{q}}_\mathbf{i}, \tag{4}$$

where $\boldsymbol{X_i} = [\,\boldsymbol{p}_{\boldsymbol{v},i}^{\boldsymbol{T}}\ \boldsymbol{\phi}_{\boldsymbol{v},i}^{\boldsymbol{T}}\,]^{\boldsymbol{T}} \in \boldsymbol{R}^6$ is the task space coordinate vector for the i*th* robot. $\boldsymbol{P_{v,i}} = [x_i\, y_i\, z_i]^{\mathrm{T}}$ and $\boldsymbol{\phi}_{\mathbf{v},\mathbf{i}} = [\alpha_i\, \beta_i\, \gamma_i]^{\mathrm{T}}$ are position and orientation of the tip of virtual links with respect to base coordinate system respectively.

2.3. Object space dynamic equations

The dynamic equation of the system in the object space could be considered as two decomposed dynamic equations, i.e. shaped and locked systems.[11,24] In centralized control of cooperative systems for object grasping and manipulation, the shaped dynamic system is the portion of the entire dynamic

https://doi.org/10.1017/S0263574714002379 Published online by Cambridge University Press

system responsible for the coordination of robots with respect to each other (i.e. to grasp the object properly and control the internal force exerted on the object). The locked dynamic system is responsible for the coordinated motion of all robots to move the object along with desired trajectory.

A decomposition matrix, $\mathbf{S}$, is proposed to decompose the task space dynamic equations of robots into object space dynamic equations. To propose a proper decomposition matrix, $\boldsymbol{X_E}$ and $\boldsymbol{X_L}$, i.e. shaped and locked systems' coordinate vectors are selected properly. $\boldsymbol{X_E}$ illustrates the arrangement of the extended robots' end effectors with respect to each other, and is contingent to the shape of the object. Theoretically, $\boldsymbol{X_E}$ is constant since the object is rigid. $\boldsymbol{X_L} \in \boldsymbol{R}^6$ shows the position and orientation of the overall system, which is associated with the position and orientation of the object. $\boldsymbol{X_E} \in \boldsymbol{R}^{12}$ is defined by relative position and orientation of the extended robots' end effectors (tips of the virtual links) as follows:

$$\boldsymbol{X_E} = \begin{pmatrix} \boldsymbol{P_{v,2}} - \boldsymbol{P_{v,1}} \\ \boldsymbol{\phi_{v,2}} - \boldsymbol{\phi_{v,1}} \\ \boldsymbol{P_{v,3}} - \boldsymbol{P_{v,2}} \\ \boldsymbol{\phi_{v,3}} - \boldsymbol{\phi_{v,2}} \end{pmatrix}, \tag{5}$$

where $\boldsymbol{P_{v,i}}$ is the position of the tip of the virtual link associated with ith robot; $\boldsymbol{\phi_{v,i}}$ is the Euler angles vector of the end effector associated with the ith robot; and $\boldsymbol{X_L}$ is defined as

$$\boldsymbol{X_L} = \begin{pmatrix} \boldsymbol{P_L} \\ \boldsymbol{\phi_L} \end{pmatrix}, \tag{6}$$

where $\boldsymbol{P_L}$ is the average position of the end effectors, and $\boldsymbol{\phi_L}$ is the Euler angles vector for the virtual link associated with the first robot ($i = 1$). These variables are defined as follows:

$$\boldsymbol{P_L} = \frac{1}{3}\left(\boldsymbol{P_{v,1}} + \boldsymbol{P_{v,2}} + \boldsymbol{P_{v,3}}\right), \tag{7}$$

$$\boldsymbol{\phi_L} = \boldsymbol{\phi}_1 = \begin{bmatrix} \alpha_1 & \beta_1 & \gamma_1 \end{bmatrix}^T. \tag{8}$$

Then the decomposition matrix, $\mathbf{S} \in \mathbf{R}^{18\times 18}$, is obtained as:

$$\begin{bmatrix} \boldsymbol{X_L} \\ \boldsymbol{X_E} \end{bmatrix} = \overbrace{\begin{bmatrix} \mathbf{(1/3)I} & \mathbf{0} & \mathbf{(1/3)I} & \mathbf{0} & \mathbf{(1/3)I} & \mathbf{0} \\ \mathbf{0} & \mathbf{I} & \mathbf{0} & \mathbf{0} & \mathbf{0} & \mathbf{0} \\ \mathbf{-I} & \mathbf{0} & \mathbf{I} & \mathbf{0} & \mathbf{0} & \mathbf{0} \\ \mathbf{0} & \mathbf{-I} & \mathbf{0} & \mathbf{I} & \mathbf{0} & \mathbf{0} \\ \mathbf{0} & \mathbf{0} & \mathbf{-I} & \mathbf{0} & \mathbf{I} & \mathbf{0} \\ \mathbf{0} & \mathbf{0} & \mathbf{0} & \mathbf{-I} & \mathbf{0} & \mathbf{I} \end{bmatrix}}^{s} \begin{bmatrix} \boldsymbol{P_{v,1}} \\ \boldsymbol{\phi_{v,1}} \\ \boldsymbol{P_{v,2}} \\ \boldsymbol{\phi_{v,2}} \\ \boldsymbol{P_{v,3}} \\ \boldsymbol{\phi_{v,3}} \end{bmatrix}, \tag{9}$$

where $\mathbf{I} \in \mathbf{R}^{3\times 3}$ is the identity matrix and $\mathbf{0} \in \mathbf{R}^{3\times 3}$ is the zero matrix.

To transform the dynamic equations of the joint space into the object space, the following transfer matrix was used:

$$\mathbf{T} = \mathbf{S}.\mathbf{J}, \tag{10}$$

where $\mathbf{J} \in \mathbf{R}^{18\times 18}$ is the Jacobian matrix of the cooperative system, and $\mathbf{S}$ is the decomposition matrix.

Using the transfer matrix $\mathbf{T}$, the dynamic equations in the object space could be obtained as[11]

$$\underbrace{\mathbf{M_L}\left(\boldsymbol{X}\right)\ddot{\boldsymbol{X}}_{\boldsymbol{L}} + \mathbf{C_L}\left(\boldsymbol{X}, \dot{\boldsymbol{X}}\right)\dot{\boldsymbol{X}}_{\boldsymbol{L}}}_{\text{Locked system dynamics}} + \underbrace{\mathbf{C_{LE}}\left(\boldsymbol{X}, \dot{\boldsymbol{X}}\right)\dot{\boldsymbol{X}}_{\boldsymbol{E}}}_{\text{Coupling}} = \boldsymbol{T_L} + \boldsymbol{F_L}, \tag{11}$$

$$\underbrace{\mathbf{M_E}\left(\boldsymbol{X}\right)\ddot{\boldsymbol{X}}_{\boldsymbol{E}} + \mathbf{C_E}\left(\boldsymbol{X}, \dot{\boldsymbol{X}}\right)\dot{\boldsymbol{X}}_{\boldsymbol{E}}}_{\text{Shaped system dynamics}} + \underbrace{\mathbf{C_{EL}}\left(\boldsymbol{X}, \dot{\boldsymbol{X}}\right)\dot{\boldsymbol{X}}_{\boldsymbol{L}}}_{\text{Coupling}} = \boldsymbol{T_E} + \boldsymbol{F_E}. \tag{12}$$

https://doi.org/10.1017/S0263574714002379 Published online by Cambridge University Press

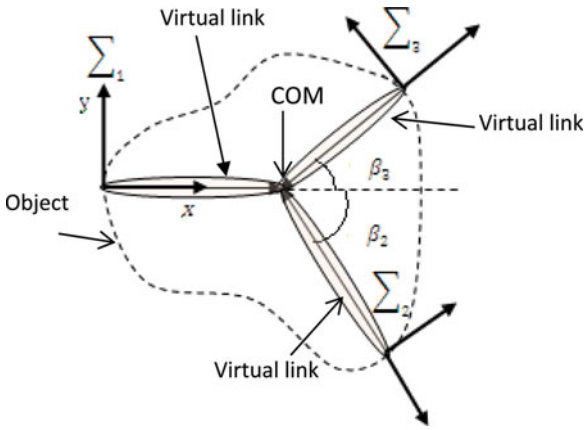


Fig. 2. Three virtual links that are connected to each other in the estimated COM.

Equations (11) and (12) are the equations of the locked and shaped systems respectively. These equations are decomposed passively such that each of the decoupled systems can be controlled independently. In Eqs. (11) and (12), $\mathbf{M_L}$ and $\mathbf{M_E}$ are the inertia matrices, $\mathbf{C_L}$ and $\mathbf{C_E}$ are the Coriolis matrices, $\mathbf{C_{LE}}$ and $\mathbf{C_{EL}}$ are the coupling terms, $\boldsymbol{T_L}$ and $\boldsymbol{T_E}$ are the control signals, and $\boldsymbol{F_L}$ and $\boldsymbol{F_E}$ are the external force in the locked and shaped systems respectively,

$$\begin{pmatrix} \mathbf{M_L}(X) & \mathbf{0} \\ \mathbf{0} & \mathbf{M_E}(X) \end{pmatrix} = \mathbf{T^{-T}} \mathrm{diag}\left\{ \mathbf{M}_1(\boldsymbol{q}_1) \quad \mathbf{M}_2(\boldsymbol{q}_2) \quad \mathbf{M}_3(\boldsymbol{q}_3) \right\} \mathbf{T}^{-1}, \tag{13}$$

$$\begin{pmatrix} \boldsymbol{T_L} \\ \boldsymbol{T_E} \end{pmatrix} = \mathbf{T^{-T}} \begin{pmatrix} \boldsymbol{\tau}_1 \\ \boldsymbol{\tau}_2 \\ \boldsymbol{\tau}_3 \end{pmatrix}, \tag{14}$$

$$\begin{pmatrix} \boldsymbol{F_L} \\ \boldsymbol{F_E} \end{pmatrix} = \mathbf{S^{-T}} \begin{pmatrix} \boldsymbol{F}_1 \\ \boldsymbol{F}_2 \\ \boldsymbol{F}_3 \end{pmatrix}, \tag{15}$$

where $\boldsymbol{F}_i$, $i = \{1,2,3\}$, is the external force exerted to the ith robot in the task space, and $\boldsymbol{\tau}_i$, $i = \{1,2,3\}$, is the vector of generalized forces of the ith robot in the joint space.

The decoupling terms, $\mathbf{C_{LE}}(\boldsymbol{X}, \dot{\boldsymbol{X}})\dot{\boldsymbol{X}}_{\boldsymbol{E}}$ and $\mathbf{C_{EL}}\boldsymbol{X}, \dot{\boldsymbol{X}})\dot{\boldsymbol{X}}_{\boldsymbol{L}}$, are obtained as follows:

$$\begin{pmatrix} \mathbf{C_L} & \mathbf{C_{LE}} \\ \mathbf{C_{EL}} & \mathbf{C_E} \end{pmatrix} = \mathbf{T^{-T}} \left(\mathbf{C_i}(\boldsymbol{q}_i, \dot{\boldsymbol{q}}_i) - \mathbf{M_i}(\boldsymbol{q}_i) \mathbf{T}^{-1} \dot{\mathbf{T}} \right) \times \mathbf{T}^{-1}. \tag{16}$$

It is supposed that the virtual links are initially located as shown in Fig. 2, and the initial values of the Euler angles for each virtual link are: $\alpha_1(\mathrm{t}_0) = 0$, $\beta_1(\mathrm{t}_0) = \beta_1$, $\gamma_1(\mathrm{t}_0) = 0$, $\alpha_2(\mathrm{t}_0) = 0$, $\beta_2(\mathrm{t}_0) = \beta_2$, $\gamma_2(\mathrm{t}_0) = 0$, $\alpha_3(\mathrm{t}_0) = 0$, $\beta_3(\mathrm{t}_0) = \beta_3$, and $\gamma_3(\mathrm{t}_0) = 0$.

Assuming that the grasped object is rigid, and using (5), the desired shaped coordinate, $\boldsymbol{X}_{\boldsymbol{E}}^{\boldsymbol{d}}$, could be obtained as:

$$\boldsymbol{X}_{\boldsymbol{E}}^{\boldsymbol{d}} = \begin{bmatrix} 0 & 0 & 0 & 0 & \hat{\beta}_2 - \hat{\beta}_1 & 0 & 0 & 0 & 0 & 0 & \hat{\beta}_3 - \hat{\beta}_2 & 0 \end{bmatrix}^T. \tag{17}$$

$\hat{\beta}_1$, $\hat{\beta}_2$, and $\hat{\beta}_3$ are the estimated values for β_1, β_2, and β_3 respectively. These estimated angles could be obtained using a proposed kinematic adaptation law, which is also used to estimate COM. In the next section, this estimation scheme is discussed.

3. The Proposed Estimation Scheme for Object's COM

Given the fact that the COM is unknown, α_i, β_i, and γ_i in the task space dynamic equations are also unknown, and hence are required to be estimated by an observer.

https://doi.org/10.1017/S0263574714002379 Published online by Cambridge University Press

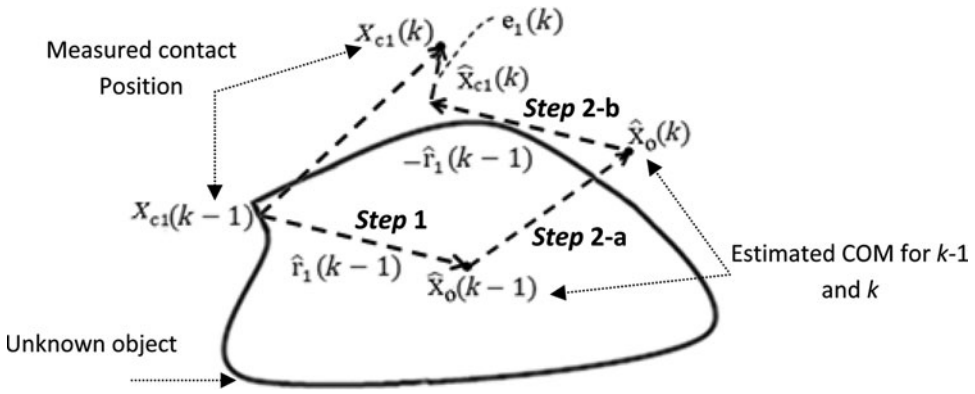


Fig. 3. Two-step iterative method for COM estimation.

A new, two-step iterative method was proposed to estimate COM.[19] In each of these two steps, COM was estimated using a different method. Estimated COM converges to the real value whenever these two steps give the same position value for COM. A new parameter observer was proposed to update the estimated virtual links as:

$$ {}^{b}\dot{\hat{\boldsymbol{r}}}_{i} = -\boldsymbol{\Gamma}_{\mathbf{i}}\boldsymbol{e}_{i} - \boldsymbol{\rho}_{i}{}^{b}\hat{\boldsymbol{r}}_{i}, \tag{18} $$

where $\boldsymbol{\Gamma}_{\mathbf{i}}$ and $\boldsymbol{\rho}_{i}$ are positive definite constant matrices for the kinematic adaptation law and its damping term respectively; ${}^{b}\hat{\boldsymbol{r}}_{i}$ is the vector that defines ith virtual link with respect to the base frame; and $\boldsymbol{e}_{i}$ is the coordinate estimation error of the ith contact point, e.g. the position error between real contact point, $\boldsymbol{X}_{ci}(k)$, and the estimated one, $\hat{\boldsymbol{X}}_{ci}(k)$, as:

$$ \boldsymbol{e}_{i} = \boldsymbol{X}_{ci}(k) - \hat{\boldsymbol{X}}_{ci}(k). \tag{19} $$

The two steps for the proposed method are as follows:

Step 1: Initial value was estimated for ${}^{b}\boldsymbol{r}_{i}(k)$ in $k = 0$, assuming a random initial position for COM. In the next iterations ($k > 0$),${}^{b}\boldsymbol{r}_{i}(k)$ is estimated using (18) after the second step ends. Having the contact position and estimated virtual link that connects the contact point to COM, the COM at $t = k$ could be obtained as shown in Fig. 3 using Eq. (20) as follows:

$$ \hat{\boldsymbol{X}}_{o_i}(k-1) = \boldsymbol{X}_{ci}(k-1) - {}^{b}\hat{\boldsymbol{r}}_{i}(k-1), \tag{20} $$

where $\hat{\boldsymbol{X}}_{o_i}$ is the estimated COM. The COM estimated by Eq. (20) is obtained considering only one robot. Now, considering the other two robots, the estimated COM is given by:

$$ \hat{\boldsymbol{X}}_{o}(\mathrm{k}-1) = (1/3)\sum_{i=1}^{3}\hat{\boldsymbol{X}}_{o_i}(\mathrm{k}-1). \tag{21} $$

Step 2a: Using the total external force vector (equal to the sum of the three contact force vectors, i.e. $\sum_{i=1}^{3}\boldsymbol{F}_{ci}$, where $\boldsymbol{F}_{ci}$ is the contact force measured by force sensor), and the object's mass, an acceleration vector could be estimated based on Newton's second law. The acceleration vector and estimated COM in the previous iteration, $\hat{\boldsymbol{X}}_{o}(k-1)$, is used to estimate the updated COM in the new iteration, $\hat{\boldsymbol{X}}_{o}(k)$, (for more details see ref. [19]). Point $\hat{\boldsymbol{X}}_{o}(\boldsymbol{k})$ is shown in Fig. 3.

Step 2b: Given the updated COM, and by incorporating $-{}^{b}\hat{\boldsymbol{r}}_{i}(k-1)$g, a new estimation for the contact point could be obtained as shown in Fig. 3,

$$ \hat{\boldsymbol{X}}_{ci}(k) = \hat{\boldsymbol{X}}_{o}(k) - {}^{b}\hat{\boldsymbol{r}}_{i}(k-1). \tag{22} $$

https://doi.org/10.1017/S0263574714002379 Published online by Cambridge University Press

Using Eqs. (19) and (22), the contact position estimation error in the next iteration is obtained as follows:

$$\boldsymbol{e_i} = \boldsymbol{X_{ci}}(k) - \left\{\hat{\boldsymbol{X}}_{\boldsymbol{o}}(k) - {}^{\boldsymbol{b}}\boldsymbol{r}_i(k-1)\right\}. \tag{23}$$

Error between the measured position for a contact point and the estimated position, $\boldsymbol{e_i}$, is substituted into Eq. (18) to calculate a new ${}^{\boldsymbol{b}}\hat{\boldsymbol{r}}_{\boldsymbol{i}}$(k). The new ${}^{\boldsymbol{b}}\hat{\boldsymbol{r}}_{\boldsymbol{i}}$ results in a reduced error ($\boldsymbol{e_i}$) in the new iteration. After completing the second step, a new iteration starts with running the first step again. These iterations continue until $\boldsymbol{e_i}$ converges to zero.

${}^{\boldsymbol{b}}\hat{\boldsymbol{r}}_{\boldsymbol{i}}$(k) is a function of $\alpha_i(k)$, $\beta_i(k)$, and $L_i(k)$. Therefore, corresponding values for $\hat{\alpha}_i(k)$, $\hat{\beta}_i(k)$, and $\hat{L}_i(k)$ could be obtained after estimating a new value for ${}^{\boldsymbol{b}}\hat{\boldsymbol{r}}_{\boldsymbol{i}}$(k) in each iteration.

4. Controller Design for Cooperative System

In this section, two controllers, $\boldsymbol{T_E}$ and $\boldsymbol{T_L}$ (i.e. control actions for the locked and shaped systems respectively) plus a damping controller are designed in the object space as follows:

$$\begin{pmatrix} \boldsymbol{T_L} \\ \boldsymbol{T_E} \end{pmatrix} = \underbrace{\begin{pmatrix} \hat{\boldsymbol{C}}_{\mathbf{LE}}(\boldsymbol{X}, \dot{\boldsymbol{X}})\dot{\boldsymbol{X}}_{\boldsymbol{E}} \\ \hat{\boldsymbol{C}}_{\mathbf{EL}}(\boldsymbol{X}, \dot{\boldsymbol{X}})\dot{\boldsymbol{X}}_{\boldsymbol{L}} \end{pmatrix}}_{Tc} + \begin{pmatrix} T'_L \\ T'_E \end{pmatrix}, \tag{24}$$

where $\hat{\mathbf{C}}_{\mathbf{LE}}(\boldsymbol{X}, \dot{\boldsymbol{X}})$ and $\hat{\mathbf{C}}_{\mathbf{EL}}(\boldsymbol{X}, \dot{\boldsymbol{X}})$ are estimated according to (16), $\boldsymbol{T_c}$ is the decoupling controller,[11,20] $\boldsymbol{T'_L}$ is a sliding-mode adaptive controller proposed for the locked system, and $\boldsymbol{T'_E}$ is a composite controller based on a PD controller plus a stabilizing damping term proposed for the shaped system. Each of these controllers are discussed as follows.

4.1. Decoupling controller

It is shown in Lee and Spong[11] and Monfaredi *et al.*[20] that $\mathbf{C_{LE}} = -\mathbf{C}^{\mathbf{T}}_{\mathbf{EL}}$. The same holds for estimated functions, i.e. $\hat{\mathbf{C}}_{\mathbf{LE}}(\boldsymbol{X}, \dot{\boldsymbol{X}}) = -\hat{\mathbf{C}}^{\mathbf{T}}_{\mathbf{EL}}(\boldsymbol{X}, \dot{\boldsymbol{X}})$. As both sides of the equality are the functions of the same arguments, the equality is true in spite of the replacement of actual parameters with their estimated values. Similar to Lee and Spong,[11] it can be shown that $\dot{\boldsymbol{X}}^{\boldsymbol{T}}_{\boldsymbol{L}}\hat{\mathbf{C}}_{\mathbf{LE}}(\boldsymbol{X}, \dot{\boldsymbol{X}})\dot{\boldsymbol{X}}_{\boldsymbol{E}} + \dot{\boldsymbol{X}}^{\boldsymbol{T}}_{\boldsymbol{E}}\hat{\mathbf{C}}_{\mathbf{LE}}(\boldsymbol{X}, \dot{\boldsymbol{X}})\dot{\boldsymbol{X}}_{\boldsymbol{L}} = 0$, hence the decoupling procedure does not generate (or dissipate) any mechanical power.

Given the decoupling control (24), the shaped and locked systems' dynamics can be expressed as:

$$\mathbf{M_L}(\boldsymbol{X})\ddot{\boldsymbol{X}}_{\boldsymbol{L}} + \mathbf{C_L}\left(\boldsymbol{X}, \dot{\boldsymbol{X}}\right)\dot{\boldsymbol{X}}_{\boldsymbol{L}} = \boldsymbol{T'}_{L} + \boldsymbol{F}_{\boldsymbol{L}}, \tag{25}$$

$$\mathbf{M_E}(\boldsymbol{X})\ddot{\boldsymbol{X}}_{\boldsymbol{E}} + \mathbf{C_E}\left(\boldsymbol{X}, \dot{\boldsymbol{X}}\right)\dot{\boldsymbol{X}}_{\boldsymbol{E}} = \boldsymbol{T'}_{E} + \boldsymbol{F}_{\boldsymbol{E}}, \tag{26}$$

where (25) is the dynamic equation of the locked system and (26) is the dynamic equation of the shaped system after incorporating decoupling controller to the system. In the following two sections, the shaped system controller and the locked system controller are developed respectively.

4.2. Shaped System Controller

The control objective of the shaped system controller is $\boldsymbol{X_E} \rightarrow \boldsymbol{X^d_E}$, where $\boldsymbol{X^d_E}$ is defined by (17).The shaped system controller is proposed as:

$$\boldsymbol{T'}_{E} = -\mathbf{K^E_d}\dot{\boldsymbol{X}}_{\boldsymbol{E}} - \mathbf{K^E_p}\left(\boldsymbol{X_E} - \boldsymbol{X^d_E}\right) + \left(\dot{\boldsymbol{X}}^{\boldsymbol{T}}_{\boldsymbol{E}}\right)^{+}\left[\boldsymbol{e}^{\boldsymbol{T}}_1 \quad \boldsymbol{e}^{\boldsymbol{T}}_2 \quad \boldsymbol{e}^{\boldsymbol{T}}_3\right]K'\begin{bmatrix} {}^{\boldsymbol{b}}\hat{\boldsymbol{r}}_1 \\ {}^{\boldsymbol{b}}\hat{\boldsymbol{r}}_2 \\ {}^{\boldsymbol{b}}\hat{\boldsymbol{r}}_3 \end{bmatrix}, \tag{27}$$

$$\left(\dot{\boldsymbol{X}}^{\boldsymbol{T}}_{\boldsymbol{E}}\right)^{+} = \left[\dot{\boldsymbol{X}}_{\boldsymbol{E}}\left(\dot{\boldsymbol{X}}^{\boldsymbol{T}}_{\boldsymbol{E}}\dot{\boldsymbol{X}}_{\boldsymbol{E}}\right)^{-1}\right],$$

https://doi.org/10.1017/S0263574714002379 Published online by Cambridge University Press

where $(\dot{\boldsymbol{X}}_{\boldsymbol{E}}^{\boldsymbol{T}})^{+}$ denotes the pseudo inverse of $\dot{\boldsymbol{X}}_{\boldsymbol{E}}^{\boldsymbol{T}}$, $\mathbf{K}' = \begin{bmatrix} \mathbf{k'}_1 & \mathbf{0} & \mathbf{0} \\ \mathbf{0} & \mathbf{k'}_2 & \mathbf{0} \\ \mathbf{0} & \mathbf{0} & \mathbf{k'}_3 \end{bmatrix} \in \mathbf{R}^{9\times 9}$ is a symmetric positive definite matrix ($\mathbf{k'_i} \in \mathbf{R}^{3\times 3}$ isalsoapositivedefinitematrix), and $\boldsymbol{e}_{\boldsymbol{i}}^{\boldsymbol{T}}$ is the contact point estimation error given by (19). The last term in (27) ensures the shaped system stability and bounded parameters for kinematic adaptation law, as is shown in Section 5. The gains $\mathbf{K_d^E}$ and $\mathbf{K_p^E}$ are symmetric positive definite matrices for the derivate and proportional gains of the shaped system controller respectively.

4.3. Locked system controller

To design the sliding-mode adaptive controller for the locked system, first the locked system dynamics are expressed in a linear-in-parameter form. Using the linear-in-parameter equation for each robot and transforming these into the object space, linear-in-parameter form of the locked system dynamics are obtained:

$$\mathbf{Y}_{\boldsymbol{ir}}\boldsymbol{\theta}_{\boldsymbol{id}} = \begin{bmatrix} -ls\alpha c\beta\ddot{\alpha}_r - lc\alpha s\beta\ddot{\beta}_r - lc\alpha c\beta\dot{\alpha}\dot{\alpha}_r + ls\alpha s\beta\dot{\beta}\dot{\alpha}_r \\ \quad - lc\alpha s\beta\dot{\beta}\dot{\beta}_r + ls\alpha s\beta\dot{\alpha}\dot{\beta}_r + \ddot{x}_r & 0 & 0 & (m_{xi} + m_{yi} + m_{zi})\ddot{x}_r \\ ls\alpha s\beta\ddot{\alpha}_r + lc\alpha c\beta\ddot{\beta}_r - lc\alpha s\beta\dot{\alpha}\dot{\alpha}_r - ls\alpha c\beta\dot{\beta}\dot{\alpha}_r \\ \quad - lc\alpha s\beta\dot{\beta}\dot{\beta}_r - ls\alpha c\beta\dot{\alpha}\dot{\beta}_r + \ddot{y}_r & 0 & 0 & (m_z + m_y)\ddot{y}_r \\ \ddot{z}_r - lc\alpha\ddot{\alpha}_r + ls\alpha\dot{\alpha}\dot{\alpha}_r + g & 0 & 0 & m_z(\ddot{z}_r + g) \\ -ls\alpha c\beta\ddot{x}_r - ls\alpha s\beta\ddot{y}_r - c\alpha\ddot{z}_r + l^2c\alpha s\alpha\dot{\beta}\dot{\beta}_r \\ \quad + l^2\ddot{\alpha}_r - glc\alpha & \ddot{\alpha}_r & 0 & 0 \\ -lc\alpha s\beta\ddot{x}_r + lc\alpha c\beta\ddot{y}_r - glc\beta + l^2c^2\alpha\ddot{\beta}_r \\ \quad - l^2\ddot{\beta}_r - 2l^2c\alpha s\alpha\dot{\beta}\dot{\alpha}_r + l^2\ddot{\beta}_r & \ddot{\beta}_r & 0 & 0 \\ 0 & 0 & \ddot{y}_r & 0 \end{bmatrix} \begin{bmatrix} \theta_{1i} \\ \theta_{2i} \\ \theta_{3i} \\ 1 \end{bmatrix}, \tag{28}$$

where $\mathbf{Y}_{\boldsymbol{ir}}$ is the regressor matrix and $\boldsymbol{\theta}_{\boldsymbol{id}}$ is the dynamic parameter vector for the ith extended robot respectively; $\theta_{1i} = m_{li}, \theta_{2i} = I_{y/zi}$, and $\theta_{3i} = I_{xi}$; and m_{xi}, m_{yi}, and m_{zi} are the mass for the x, y, and z links of the ith robot respectively.

$$\begin{pmatrix} \dot{\boldsymbol{q}}_{1r} \\ \dot{\boldsymbol{q}}_{2r} \\ \dot{\boldsymbol{q}}_{3r} \end{pmatrix} = \mathbf{J}^{-1}\mathbf{S}^{-1} \begin{pmatrix} \dot{\boldsymbol{X}}_{\boldsymbol{Lr}} \\ \dot{\boldsymbol{X}}_{\boldsymbol{Er}} \end{pmatrix}, \tag{29}$$

where $\dot{\boldsymbol{X}}_{\boldsymbol{Lr}}$ and $\dot{\boldsymbol{X}}_{\boldsymbol{Er}}$ are the reference velocities for the locked and shaped systems respectively; And $\dot{\boldsymbol{q}}_{\boldsymbol{ir}} = [\,\dot{x}_{ir}\ \dot{y}_{ir}\ \dot{z}_{ir}\ \dot{\alpha}_{ir}\ \dot{\beta}_{ir}\ \dot{\gamma}_{ir}\,]^T$ is the ith robot's reference velocity in the joint space. Taking the time derivative of (29), the following is obtained:

$$\begin{pmatrix} \ddot{\boldsymbol{q}}_{1r} \\ \ddot{\boldsymbol{q}}_{2r} \\ \ddot{\boldsymbol{q}}_{3r} \end{pmatrix} = \mathbf{J}^{-1}\mathbf{S}^{-1} \begin{pmatrix} \ddot{\boldsymbol{X}}_{\boldsymbol{Lr}} \\ \ddot{\boldsymbol{X}}_{\boldsymbol{Er}} \end{pmatrix} + \dot{\mathbf{J}}^{-1}\mathbf{S}^{-1} \begin{pmatrix} \dot{\boldsymbol{X}}_{\boldsymbol{Lr}} \\ \dot{\boldsymbol{X}}_{\boldsymbol{Er}} \end{pmatrix}, \tag{30}$$

where

$$\mathbf{J}^{-1} = -\mathbf{J}^{-1}\mathbf{J}\mathbf{J}^{-1}, \tag{31}$$

$$\mathrm{J}^{-1} = \begin{bmatrix} \mathrm{J}_1^{-1} & 0 & 0 \\ 0 & \mathrm{J}_2^{-1} & 0 \\ 0 & 0 & \mathrm{J}_3^{-1} \end{bmatrix}, \tag{32}$$

$\dot{\mathbf{J}}$ is the time derivative of the cooperative system's Jacobian matrix,
and

$$\dot{\boldsymbol{X}}_{\boldsymbol{Lr}} = \dot{\boldsymbol{X}}_{\boldsymbol{Ld}} - \boldsymbol{\lambda}_2\boldsymbol{e}_{\boldsymbol{L}}, \tag{33}$$

https://doi.org/10.1017/S0263574714002379 Published online by Cambridge University Press

$$\ddot{\boldsymbol{X}}_{\boldsymbol{Lr}} = \ddot{\boldsymbol{X}}_{\boldsymbol{Ld}} - \boldsymbol{\lambda}_1 \dot{\boldsymbol{e}}_{\boldsymbol{L}}, \tag{34}$$

$$\dot{\boldsymbol{X}}_{\boldsymbol{Er}} = \dot{\boldsymbol{X}}_{\boldsymbol{Ed}} - \boldsymbol{\lambda}_2 \boldsymbol{e}_{\boldsymbol{E}}, \tag{35}$$

$$\dot{\boldsymbol{X}}_{\boldsymbol{Er}} = \dot{\boldsymbol{X}}_{\boldsymbol{Ed}} - \boldsymbol{\lambda}_1 \dot{\boldsymbol{e}}_{\boldsymbol{E}}, \tag{36}$$

where $\dot{\boldsymbol{X}}_{\boldsymbol{Ld}}$ and $\ddot{\boldsymbol{X}}_{\boldsymbol{Ld}}$ are the desired velocity and acceleration vectors for the locked system, and $\dot{\boldsymbol{X}}_{\boldsymbol{Ed}} = 0$ and $\ddot{\boldsymbol{X}}_{\boldsymbol{Ed}} = 0$ are the desired velocity and acceleration vectors for the shaped system respectively; $\ddot{\boldsymbol{X}}_{\boldsymbol{Lr}}$ and $\ddot{\boldsymbol{X}}_{\boldsymbol{Er}}$ are the reference acceleration vectors for the locked and shaped systems respectively; $\boldsymbol{e}_{\boldsymbol{L}}$ and $\boldsymbol{e}_{\boldsymbol{E}}$ are the closed-loop error vectors for the locked and shaped systems respectively; and $\boldsymbol{\lambda}_1$ and $\boldsymbol{\lambda}_2$ are positive definite constant matrices. To get a linear-in-parameter dynamics for locked and shaped systems, the following change in variables is proposed:

$$\begin{bmatrix} \mathbf{T}'_{\boldsymbol{L}} \\ \mathbf{T}'_{\boldsymbol{E}} \end{bmatrix} = \mathbf{S}^{-\boldsymbol{T}} \mathbf{J}^{-\boldsymbol{T}} \begin{bmatrix} \boldsymbol{\tau}_1 \\ \boldsymbol{\tau}_2 \\ \boldsymbol{\tau}_3 \end{bmatrix}. \tag{37}$$

Using the same transformation as (37), the linear-in-parameter dynamics of the robots could be transformed into the object space as:

$$\mathbf{Y}_{\mathbf{or}} \boldsymbol{\theta}_{\boldsymbol{od}} = \begin{bmatrix} \mathbf{Y}_{\mathbf{Lr}} \boldsymbol{\theta}_{\boldsymbol{Ld}} \\ \mathbf{Y}_{\mathbf{Er}} \boldsymbol{\theta}_{\boldsymbol{Ed}} \end{bmatrix} = \mathbf{S}^{-\mathbf{T}} \mathbf{J}^{-\mathbf{T}} \begin{bmatrix} \mathbf{Y}_{\mathbf{1r}} \boldsymbol{\theta}_{\mathbf{1}\boldsymbol{d}} \\ \mathbf{Y}_{\mathbf{2r}} \boldsymbol{\theta}_{\mathbf{2}\boldsymbol{d}} \\ \mathbf{Y}_{\mathbf{3r}} \boldsymbol{\theta}_{\mathbf{3}\boldsymbol{d}} \end{bmatrix} = \mathbf{S}^{-\mathbf{T}} \mathbf{J}^{-\mathbf{T}} \mathbf{diag}\{ \mathbf{Y}_{\mathbf{1r}} \quad \mathbf{Y}_{\mathbf{2r}} \quad \mathbf{Y}_{\mathbf{3r}} \} \begin{bmatrix} \boldsymbol{\theta}_{\mathbf{1}\boldsymbol{d}} \\ \boldsymbol{\theta}_{\mathbf{2}\boldsymbol{d}} \\ \boldsymbol{\theta}_{\mathbf{3}\boldsymbol{d}} \end{bmatrix}, \tag{38}$$

$$\mathbf{Y}_{\mathbf{or}} = \mathbf{S}^{-\boldsymbol{T}} \mathbf{J}^{-\boldsymbol{T}} \mathbf{diag}\{ \mathbf{Y}_{\mathbf{1r}} \quad \mathbf{Y}_{\mathbf{2r}} \quad \mathbf{Y}_{\mathbf{3r}} \}, \tag{39}$$

where $\mathbf{Y}_{\mathbf{or}}$ is the regressor matrix of the overall system in the object space and $\boldsymbol{\theta}_{\boldsymbol{od}}$ is the dynamic parameter vector of the overall system defined as:

$$\boldsymbol{\theta}_{\boldsymbol{od}} = \begin{bmatrix} \boldsymbol{\theta}_{\mathbf{1}\boldsymbol{d}} \\ \boldsymbol{\theta}_{\mathbf{2}\boldsymbol{d}} \\ \boldsymbol{\theta}_{\mathbf{3}\boldsymbol{d}} \end{bmatrix} = \begin{bmatrix} m_1 & I_{z/y1} & I_{x1} & 1 & m_2 & I_{y/z2} & I_{x2} & 1 & m_2 & I_{z/y3} & I_{x3} & 1 \end{bmatrix}^T, \tag{40}$$

Using (35) and (36) to derive the regressor matrix of the shaped and locked system yields the following equations:

$$\mathbf{Y}_{\mathbf{Lr}} \boldsymbol{\theta}_{\boldsymbol{Ld}} = \begin{bmatrix} \mathbf{I}^{6\times 6} & 0^{6\times 12} \end{bmatrix} \mathbf{Y}_{\mathbf{or}} \boldsymbol{\theta}_{\mathbf{od}}, \tag{41}$$

$$\mathbf{Y}_{\mathbf{Er}} \boldsymbol{\theta}_{\boldsymbol{Ed}} = \begin{bmatrix} 0^{12\times 6} & \mathbf{I}^{12\times 12} \end{bmatrix} \mathbf{Y}_{\mathbf{or}} \boldsymbol{\theta}_{\boldsymbol{od}}, \tag{42}$$

$$\mathbf{Y}_{\mathbf{Lr}} = \begin{bmatrix} \mathbf{I}^{6\times 6} & 0^{6\times 12} \end{bmatrix} \mathbf{Y}_{\mathbf{or}}, \tag{43}$$

$$\mathbf{Y}_{\mathbf{Er}} = \begin{bmatrix} 0^{12\times 6} & \mathbf{I}^{12\times 12} \end{bmatrix} \mathbf{Y}_{\mathbf{or}}, \tag{44}$$

$$\hat{\boldsymbol{\theta}}_{\boldsymbol{Ld}} = \hat{\boldsymbol{\theta}}_{\boldsymbol{od}} = \begin{bmatrix} \hat{m}_1 & \hat{I}_{y/z1} & \hat{I}_{x1} & 1 & \hat{m}_2 & \hat{I}_{y/z2} & \hat{I}_{x2} & 1 & \hat{m}_3 & \hat{I}_{y/z3} & \hat{I}_{x3} & 1 \end{bmatrix}^T, \tag{45}$$

$\mathbf{Y}_{\mathbf{Lr}}$ and $\mathbf{Y}_{\mathbf{Er}}$ are the regressor matrices for locked and shaped systems, respectively; $\boldsymbol{\theta}_{\boldsymbol{Ld}}$ is the dynamic parameter vector of the locked system; $\hat{\boldsymbol{\theta}}_{\boldsymbol{Ld}}$ is the estimation of $\boldsymbol{\theta}_{\boldsymbol{Ld}}$, which is unknown and should be estimated using a dynamic adaptation law proposed in Section 5.

Now consider $\boldsymbol{s}_{\boldsymbol{L}} = \dot{\boldsymbol{e}}_{\boldsymbol{L}} + \lambda \boldsymbol{e}_{\boldsymbol{L}}$ as a sliding vector, the sliding-mode adaptive controller for the locked system is proposed as follows:

$$\hat{\boldsymbol{s}}_{\boldsymbol{L}} = \hat{\dot{\boldsymbol{X}}}_{\boldsymbol{L}} - \hat{\dot{\boldsymbol{X}}}_{\boldsymbol{Lr}}, \tag{46}$$

$$\hat{\hat{\boldsymbol{s}}}_{\boldsymbol{L}} = \hat{\dot{\boldsymbol{X}}}_{\boldsymbol{L}} - \hat{\dot{\boldsymbol{X}}}_{\boldsymbol{Lr}}, \tag{47}$$

https://doi.org/10.1017/S0263574714002379 Published online by Cambridge University Press

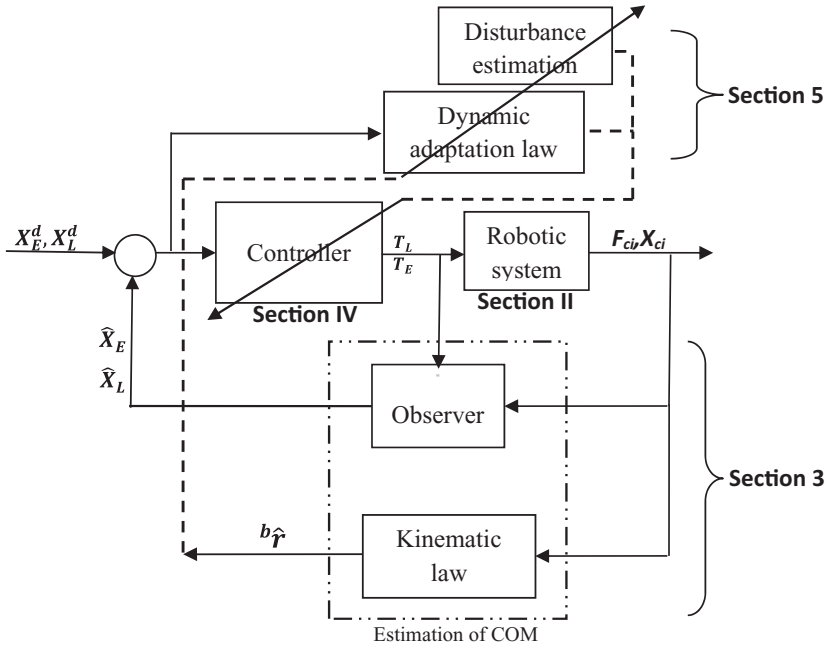


Fig. 4. Block diagram of the closed-loop system.

where $\hat{s}_L$ and $\hat{\dot{s}}_L$ are the estimations for s_L and $\dot{s}_L$ respectively. The observer-based model of the locked system is considered as:

$$\hat{\mathbf{M}}_{\mathbf{L}}\left(\hat{X}\right)\ddot{X}_L + \hat{\mathbf{C}}_{\mathbf{L}}\left(\hat{X}, \hat{\dot{X}}\right)\dot{X}_L = T'_L + F_L. \tag{48}$$

Moreover, the linear-in-parameter form of the reference model is given by

$$\hat{\mathbf{M}}_{\mathbf{L}}\left(\hat{X}\right)\ddot{X}_{Lr} + \hat{C}_L\left(\hat{X}, \hat{\dot{X}}\right)\dot{X}_{Lr} = \hat{Y}_{\mathbf{Lr}}\theta_{Ld}, \tag{49}$$

where $\hat{Y}_{\mathbf{Lr}}$ is the estimation of $\mathbf{Y_{Lr}}$. Subtracting (49) from (48), the locked system dynamic equation is obtained as:

$$\hat{\mathbf{M}}_{\mathbf{L}}(X)\hat{\dot{s}}_L + \hat{\mathbf{C}}_{\mathbf{L}}\left(X, \dot{X}\right)\hat{s}_L = T'_L + F_L - \hat{Y}_{\mathbf{Lr}}\theta_{Ld}. \tag{50}$$

The following controller is proposed for the locked system:

$$T'_L = -\mathbf{k_d}\hat{s}_L - \mathbf{k}e_L + \hat{Y}_{\mathbf{Lr}}\hat{\theta}_{Ld} - \hat{F}_L, \tag{51}$$

where $\mathbf{k_d}$ and $\mathbf{k}$ are the positive definite constant matrices, and $\hat{\theta}_{Ld}$ and $\hat{F}_L$ are the estimations of θ_{Ld} and F_L respectively. Substituting (51) into (50), the locked system closed loop dynamics' equation is given by:

$$\hat{\mathbf{M}}_{\mathbf{L}}(X)\hat{\dot{s}}_L + \hat{\mathbf{C}}_{\mathbf{L}}\left(X, \dot{X}\right)\hat{s}_L = \hat{Y}_{\mathbf{Lr}}\tilde{\theta}_{Ld} - \mathbf{K_L^d}\hat{s}_L + \tilde{F}_L, \tag{52}$$

where $\tilde{F}_L = F_L - \hat{F}_L$, and $\tilde{\theta}_{Ld} = \theta_{Ld} - \hat{\theta}_{Ld}$. In the following section, the stability of the cooperative system is discussed and the proper dynamic adaptation law has been selected. The schematic of the closed-loop system is illustrated in Fig. 4. Each part of this schematic is discussed in the section and is labeled.

https://doi.org/10.1017/S0263574714002379 Published online by Cambridge University Press

5. Stability Analysis

This section contains a mathematical proof of stability for the proposed controllers, based on the passivity theory. First, it is shown that the stability of shaped and locked systems ensures the stability of the entire system. Then the stability of shaped and locked systems are shown separately.

The supply rate of the cooperative system comprising three robots is obtained as follows:

$$s\left(\dot{\boldsymbol{q}}_1, \dot{\boldsymbol{q}}_2, \dot{\boldsymbol{q}}_3, \boldsymbol{F}_1, \boldsymbol{F}_2, \boldsymbol{F}_3\right) = \boldsymbol{F}_1^T \dot{\boldsymbol{q}}_1 + \boldsymbol{F}_2^T \dot{\boldsymbol{q}}_2 + \boldsymbol{F}_3^T \dot{\boldsymbol{q}}_3. \tag{53}$$

Passivity condition of the closed-loop control system is given by[25]

$$\int_0^t s\left(\dot{\boldsymbol{q}}_1(\boldsymbol{\tau}), \dot{\boldsymbol{q}}_2(\boldsymbol{\tau}), \dot{\boldsymbol{q}}_3(\boldsymbol{\tau}), \mathbf{F}_1(\boldsymbol{\tau}), \mathbf{F}_2(\boldsymbol{\tau}), \mathbf{F}_3(\boldsymbol{\tau})\right) d\boldsymbol{\tau} \geq -c^2, \ \forall t \geq 0. \tag{54}$$

The supply rate defined in (53) inspires the following definition for the kinetic energy of the cooperative system:

$$V\left(\dot{\boldsymbol{q}}_1, \dot{\boldsymbol{q}}_2, \dot{\boldsymbol{q}}_3\right) = \frac{1}{2}\dot{\boldsymbol{q}}_1^T \mathbf{M}_1 \dot{\boldsymbol{q}}_1 + \frac{1}{2}\dot{\boldsymbol{q}}_2^T \mathbf{M}_2 \dot{\boldsymbol{q}}_2 + \frac{1}{2}\dot{\boldsymbol{q}}_3^T \mathbf{M}_3 \dot{\boldsymbol{q}}_3. \tag{55}$$

Using the coordinate transformation, the kinetic energy (55) is the sum of the kinetic energies of shaped and locked systems,

$$V\left(\dot{\boldsymbol{q}}_1, \dot{\boldsymbol{q}}_2, \dot{\boldsymbol{q}}_3\right) = \frac{1}{2}\dot{\boldsymbol{X}}_{\boldsymbol{L}}^T \mathbf{M}_{\mathbf{L}} \dot{\boldsymbol{X}}_{\boldsymbol{L}} + \frac{1}{2}\dot{\boldsymbol{X}}_{\boldsymbol{E}}^T \mathbf{M}_{\mathbf{E}} \dot{\boldsymbol{X}}_{\boldsymbol{E}}. \tag{56}$$

Moreover, because of coordinate transformation, the supply rate in (53) is the sum of the usual individual supply rates of locked and shaped systems, i.e.

$$s\left(\dot{\boldsymbol{q}}_1, \dot{\boldsymbol{q}}_2, \dot{\boldsymbol{q}}_3, \boldsymbol{F}_1, \boldsymbol{F}_2, \boldsymbol{F}_3\right) = \boldsymbol{F}_{\boldsymbol{L}}^T \dot{\boldsymbol{X}}_{\boldsymbol{L}} + \boldsymbol{F}_{\boldsymbol{E}}^T \dot{\boldsymbol{X}}_{\boldsymbol{E}}. \tag{57}$$

According to Lee and Spong,[11] the cooperative system is passive if each of the decomposed locked and shaped systems are individually passive. In other words:

$$\int_0^t \boldsymbol{F}_{\boldsymbol{L}}^T \dot{\boldsymbol{X}}_{\boldsymbol{L}} dt \geq -c_L^2, \text{ and } \int_0^t \boldsymbol{F}_{\boldsymbol{E}}^T \dot{\boldsymbol{X}}_{\boldsymbol{E}} dt \geq -c_E^2. \tag{58}$$

In the following two sections, the stability of shaped and locked systems are discussed separately.

5.1. Stability of shaped system

The *shaped* system dynamics due to decomposition is as follows:

$$\mathbf{M}_{\mathbf{E}}(\boldsymbol{X})\ddot{\boldsymbol{X}}_{\boldsymbol{E}} + \mathbf{C}_{\mathbf{E}}\left(\boldsymbol{X}, \dot{\boldsymbol{X}}\right)\dot{\boldsymbol{X}}_{\boldsymbol{E}} = \boldsymbol{T}_{\boldsymbol{E}} + \boldsymbol{F}_{\boldsymbol{E}}. \tag{59}$$

The following energy function for the *shaped* system is defined:

$$V_E = \frac{1}{2}\begin{bmatrix} \boldsymbol{X}_{\boldsymbol{E}}^T & \dot{\boldsymbol{X}}_{\boldsymbol{E}}^T & {}^b\hat{\boldsymbol{r}}_1^T & {}^b\hat{\boldsymbol{r}}_2^T & {}^b\hat{\boldsymbol{r}}_3^T \end{bmatrix} \mathbf{M} \begin{bmatrix} \boldsymbol{X}_{\boldsymbol{E}} \\ \dot{\boldsymbol{X}}_{\boldsymbol{E}} \\ {}^b\hat{\boldsymbol{r}}_1 \\ {}^b\hat{\boldsymbol{r}}_2 \\ {}^b\hat{\boldsymbol{r}}_3 \end{bmatrix}, \tag{60}$$

https://doi.org/10.1017/S0263574714002379 Published online by Cambridge University Press

where $\mathbf{M} \in \mathbf{R}^{36\times 36}$ is defined as follows:

$$\mathbf{M} = \begin{bmatrix} \mathbf{K_p^E} & \mathbf{A} & \mathbf{A} & \mathbf{A} & \mathbf{A} \\ \mathbf{A} & \mathbf{M_E} & \mathbf{A} & \mathbf{A} & \mathbf{A} \\ \mathbf{A} & \mathbf{A} & \mathbf{k}_1 & \mathbf{B} & \mathbf{B} \\ \mathbf{A} & \mathbf{A} & \mathbf{B} & \mathbf{k}_2 & \mathbf{B} \\ \mathbf{A} & \mathbf{A} & \mathbf{B} & \mathbf{B} & \mathbf{k}_3 \end{bmatrix}, \tag{61}$$

where $\mathbf{A} = \mathbf{0} \in \mathbf{R}^{12\times 12}$ and $\mathbf{B} = \mathbf{0} \in \mathbf{R}^{3\times 3}$, and $\mathbf{k}_1$, $\mathbf{k}_2$, and $\mathbf{k}_3$ are positive definite matrices selected such that:

$$\mathbf{k'_i} - \mathbf{\Gamma_i^T k_i} = 0, \quad i = \{1, 2, 3\}. \tag{62}$$

$\mathbf{\Gamma_i}$ and $\mathbf{k'_i}$ are positive definite constant matrices defined in (18) and (27) respectively.

Using the skew symmetric property of $\dot{\mathbf{M}}_\mathbf{E} - 2\mathbf{C_E}$, the following can be obtained:

$$\dot{V}_E = \dot{\boldsymbol{X}}_E^T \mathbf{K_p^E} \boldsymbol{X}_E + \dot{\boldsymbol{X}}_E^T \mathbf{M_E} \ddot{\boldsymbol{X}}_E + \dot{\boldsymbol{X}}_E^T \dot{\mathbf{M}}_\mathbf{E} \dot{\boldsymbol{X}}_E + {}^b\hat{\boldsymbol{r}}_1^T \mathbf{k}_1 {}^b\dot{\hat{\boldsymbol{r}}}_1^T + {}^b\hat{\boldsymbol{r}}_2^T \mathbf{k}_2 {}^b\dot{\hat{\boldsymbol{r}}}_2^T + {}^b\hat{\boldsymbol{r}}_3^T \mathbf{k}_3 {}^b\dot{\hat{\boldsymbol{r}}}_3^T. \tag{63}$$

Now, by substituting (18) and (26) into (63) gives:

$$\begin{aligned} \dot{V}_E = {} & \dot{\boldsymbol{X}}_E^T \mathbf{K_p^E} \boldsymbol{X}_E + \dot{\boldsymbol{X}}_E^T \left[\boldsymbol{T}_E + \boldsymbol{F}_E - \mathbf{C_E}\left(X, \dot{X}\right) \dot{\boldsymbol{X}}_E \right] + \frac{1}{2} \dot{\boldsymbol{X}}_E^T \dot{\mathbf{M}}_\mathbf{E} \dot{\boldsymbol{X}}_E + \left[-\boldsymbol{e}_1^T \mathbf{\Gamma}_1^T - {}^b\hat{\boldsymbol{r}}_1^T \boldsymbol{\rho}_1^\mathbf{T} \right] \mathbf{k}_1 {}^b\dot{\hat{\boldsymbol{r}}}_1 \\ & + \left[-\boldsymbol{e}_2^T \mathbf{\Gamma}_2^T - {}^b\hat{\boldsymbol{r}}_2^T \boldsymbol{\rho}_2^\mathbf{T} \right] \mathbf{k}_2 {}^b\dot{\hat{\boldsymbol{r}}}_2 + \left[-\boldsymbol{e}_3^T \mathbf{\Gamma}_3^T - {}^b\hat{\boldsymbol{r}}_3^T \boldsymbol{\rho}_3^\mathbf{T} \right] \mathbf{k}_3 {}^b\dot{\hat{\boldsymbol{r}}}_3. \end{aligned} \tag{64}$$

Next, by substituting the shaped system control law (27) into (64), and by algebraic manipulation, the following equation is obtained:

$$\begin{aligned} \dot{V}_E = {} & -\dot{\boldsymbol{X}}_E^T \mathbf{K_d^E} \dot{\boldsymbol{X}}_E - {}^b\hat{\boldsymbol{r}}_1^T \boldsymbol{\rho}_1^\mathbf{T} \mathbf{k}_1 {}^b\dot{\hat{\boldsymbol{r}}}_1 - {}^b\hat{\boldsymbol{r}}_2^T \boldsymbol{\rho}_2^\mathbf{T} \mathbf{k}_2 {}^b\dot{\hat{\boldsymbol{r}}}_2 - {}^b\hat{\boldsymbol{r}}_3^T \boldsymbol{\rho}_3^\mathbf{T} \mathbf{k}_3 {}^b\dot{\hat{\boldsymbol{r}}}_3 + \boldsymbol{e}_1^T \left(\mathbf{k'}_1 - \mathbf{\Gamma}_1^\mathbf{T} \mathbf{k}_1 \right) {}^b\dot{\hat{\boldsymbol{r}}}_1 \\ & + \boldsymbol{e}_2^T \left(\mathbf{k'}_2 - \mathbf{\Gamma}_2^\mathbf{T} \mathbf{k}_2 \right) {}^b\dot{\hat{\boldsymbol{r}}}_2 + \boldsymbol{e}_3^T \left(\mathbf{k'}_3 - \mathbf{\Gamma}_3^\mathbf{T} \mathbf{k}_3 \right) {}^b\dot{\hat{\boldsymbol{r}}}_3 + \dot{\boldsymbol{X}}_E^T \boldsymbol{F}_E. \end{aligned} \tag{65}$$

Now substituting (62) into (65) results in:

$$\dot{V}_E = -\dot{\boldsymbol{X}}_E^T \mathbf{K_d^E} \dot{\boldsymbol{X}}_E - {}^b\hat{\boldsymbol{r}}_1^T \boldsymbol{\rho}_1^\mathbf{T} \mathbf{k}_1 {}^b\dot{\hat{\boldsymbol{r}}}_1 - {}^b\hat{\boldsymbol{r}}_2^T \boldsymbol{\rho}_2^\mathbf{T} \mathbf{k}_2 {}^b\dot{\hat{\boldsymbol{r}}}_2 - {}^b\hat{\boldsymbol{r}}_3^T \boldsymbol{\rho}_3^\mathbf{T} \mathbf{k}_3 {}^b\dot{\hat{\boldsymbol{r}}}_3 + \dot{\boldsymbol{X}}_E^T \boldsymbol{F}_E \leq \dot{\boldsymbol{X}}_E^T \boldsymbol{F}_E. \tag{66}$$

Then by integrating both sides of (66), the following equation can be obtained:

$$-V_E(0) \leq V_E(t) - V_E(0) \leq \int_0^t \dot{\boldsymbol{X}}_E^T \boldsymbol{F}_E d\tau. \tag{67}$$

Therefore, the shaped system controller guarantees the passivity of shaped system.

5.2. Stability of locked system

The following function is considered as a Lyapunov function candidate for the locked system:

$$V_L = \frac{1}{2} \left[\hat{\boldsymbol{s}}_L^T \hat{\mathbf{M}} \hat{\boldsymbol{s}}_L + \boldsymbol{e}_L^T \mathbf{k}^\mathbf{T} \boldsymbol{e}_L + \tilde{\boldsymbol{\theta}}_{Ld}^T \mathbf{\Gamma}_\mathbf{L}^{-1} \tilde{\boldsymbol{\theta}}_{Ld} + \tilde{\boldsymbol{F}}_L^T \mathbf{P} \tilde{\boldsymbol{F}}_L \right], \tag{68}$$

where $\mathbf{k}$, $\mathbf{\Gamma_L}$, and $\mathbf{P}$ are positive definite constant matrices. Differentiating (68) with respect to time, using (51), (52), and the skew symmetric property of $\dot{\mathbf{M}}_\mathbf{L} - 2\mathbf{C_L}$ for the locked system, some algebraic manipulation yields the following equations:

$$\dot{V}_L = \hat{\boldsymbol{s}}_L^T \hat{\mathbf{M}} \dot{\hat{\boldsymbol{s}}}_L + \hat{\boldsymbol{e}}_L^T \mathbf{k}^\mathbf{T} \dot{\hat{\boldsymbol{e}}}_L + \frac{1}{2} \hat{\boldsymbol{s}}_L^T \dot{\hat{\boldsymbol{M}}} \hat{\boldsymbol{s}}_L + \dot{\tilde{\boldsymbol{\theta}}}_{Ld}^\mathbf{T} \mathbf{\Gamma}_\mathbf{L}^{-1} \tilde{\boldsymbol{\theta}}_{Ld} + \dot{\tilde{\boldsymbol{F}}}_L^T \boldsymbol{P} \tilde{F}_L, \tag{69}$$

$$\dot{V}_L = \hat{\boldsymbol{s}}_L^T \left(\hat{\boldsymbol{Y}}_{\mathbf{Lr}} \tilde{\boldsymbol{\theta}}_{Ld} - \mathbf{k_d} \hat{\boldsymbol{s}}_L + \tilde{\boldsymbol{F}}_L \right) - \boldsymbol{\lambda} \hat{\boldsymbol{e}}_L^T \mathbf{k} \hat{\boldsymbol{e}}_L + \dot{\tilde{\boldsymbol{\theta}}}_{Ld}^T \mathbf{\Gamma}_\mathbf{L}^{-1} \tilde{\boldsymbol{\theta}}_{Ld} + \dot{\tilde{\boldsymbol{F}}}_L^T \mathbf{P} \tilde{\boldsymbol{F}}_L. \tag{70}$$

https://doi.org/10.1017/S0263574714002379 Published online by Cambridge University Press

Then the dynamic adaptation law is selected as:

$$\dot{\hat{\boldsymbol{\theta}}}_{Ld} = -\boldsymbol{\Gamma}_{\mathbf{L}}^{\mathbf{T}}(\hat{\boldsymbol{Y}}_{\mathbf{Lr}})^{T}\hat{\boldsymbol{s}}_{L}. \tag{71}$$

Moreover, disturbance estimator for the external force of locked system is obtained as:

$$\dot{\hat{\boldsymbol{F}}}_{L} = -\mathbf{P}^{-\mathbf{T}}\hat{\boldsymbol{s}}_{L}. \tag{72}$$

Using the above adaptation law and disturbance estimator, the following can be concluded:

$$\dot{V}_{L} = -\hat{\boldsymbol{s}}_{L}^{T}\mathbf{k}_{\mathbf{d}}\hat{\boldsymbol{s}}_{L} - \boldsymbol{\lambda}\hat{\boldsymbol{e}}_{L}^{T}\mathbf{k}\hat{\boldsymbol{e}}_{L} \leq \mathbf{0}. \tag{73}$$

Then it can be concluded that the locked system's states are bounded. Using Barbalat's lemma and showing that $\ddot{V}_L$ is bounded, it can be shown that the locked system errors converge to zero asymptotically:

$$\ddot{V}_{L} = -\dot{\hat{\boldsymbol{s}}}_{L}^{T}\mathbf{k}_{\mathbf{d}}\hat{\boldsymbol{s}}_{L} - \lambda\dot{\hat{\boldsymbol{e}}}_{L}^{T}\mathbf{k}\hat{\boldsymbol{e}}_{L}. \tag{74}$$

Equation (74) is a function of $\hat{\boldsymbol{e}}_L$, $\dot{\hat{\boldsymbol{e}}}_L^T$, $\hat{\boldsymbol{s}}_L$, and $\dot{\hat{\boldsymbol{s}}}_L^T$. According to (73), $\hat{\boldsymbol{e}}_L$ and $\hat{\boldsymbol{s}}_L$ are bounded. Concluding the boundedness of $\dot{\hat{\boldsymbol{e}}}_L$ from bounded $\hat{\boldsymbol{e}}_L$ and $\hat{\boldsymbol{s}}_L$, it is only necessary to show that $\dot{\hat{\boldsymbol{s}}}_L^T$ is bounded. Given that $\boldsymbol{X}_L^d$, $\dot{\boldsymbol{X}}_L^d$, and $\ddot{\boldsymbol{X}}_L^d$ are bounded, (47) defines that the boundedness of $\dot{\hat{\boldsymbol{s}}}_L^T$ depends on the bounded $\ddot{\hat{\boldsymbol{X}}}_L$. The bounded $\ddot{\hat{\boldsymbol{X}}}_L$ is ensured by the following; using (25), $\ddot{\hat{\boldsymbol{X}}}_L$ can be obtained as:

$$\ddot{\hat{\boldsymbol{X}}}_{L} = \mathbf{M}_{\mathbf{L}}^{-1}(\mathbf{X})\left[-\mathbf{C}_{\mathbf{L}}\left(\mathbf{X}, \dot{\boldsymbol{X}}\right)\dot{\boldsymbol{X}}_{L} + \boldsymbol{T}'_{L} + \boldsymbol{F}_{L}\right]. \tag{75}$$

Substituting the locked system controller (51) into (75) gives:

$$\ddot{\hat{\boldsymbol{X}}}_{L} = \mathbf{M}_{\mathbf{L}}^{-1}(\mathbf{X})\left[-\mathbf{C}_{\mathbf{L}}\left(\mathbf{X}, \dot{\boldsymbol{X}}\right)\dot{\boldsymbol{X}}_{L} - \mathbf{k}_{\mathbf{d}}\hat{\boldsymbol{s}}_{L} - \mathbf{k}\hat{\boldsymbol{e}}_{L} + \hat{\boldsymbol{Y}}_{\mathbf{Lr}}\hat{\boldsymbol{\theta}}_{Ld} - \tilde{\boldsymbol{F}}_{L}\right]. \tag{76}$$

According to the bounded $\dot{\boldsymbol{e}}_L$ and $\boldsymbol{e}_L$, it is concluded that $\dot{\boldsymbol{X}}_L$ and $\boldsymbol{X}_L$ are bounded. According to the boundedness of $\boldsymbol{X}_E^T$, $\dot{\boldsymbol{X}}_E$, $\boldsymbol{X}_L$, and $\dot{\boldsymbol{X}}_L$ and using (5) to (8), it is known that $\boldsymbol{X}$ and $\dot{\boldsymbol{X}}$ are bounded. $\tilde{\boldsymbol{F}}_L$ and $\hat{\boldsymbol{\theta}}_{Ld}$ are also bounded according to (74). It can also be shown that $\hat{\boldsymbol{Y}}_{\mathbf{Lr}}$ is bounded. Then $\ddot{V}_L$ is bounded and it concludes that the locked system is stable and error converges to zero asymptotically.

6. Simulation Results

In this section, the performance of the control system developed in previous sections is evaluated by simulations performed in the Matlab/Simulink environment using the SimMechanics toolbox. The robots considered in this work are 6-DOF robots. Each robot has three Cartesian and three revolute degrees of freedom. It is assumed that the contacts between finger ends and the object surface are rigid. A schematic of the considered robot is shown in Fig. 5.

As shown in Fig. 6, the object is modeled by three virtual links using the SimMechanics toolbox. Each virtual link is connected rigidly to its corresponding robot. In Fig. 6, each robot is shown with a triangle.

Three virtual links are modeled with a body block and connected rigidly to each other by a weldJoint in SimMechanics toolbox. The Cartesian degrees of freedom, x, y, and z of each robot are modeled by prismatic joints. Revolute joints of robots are modeled by gimbal joint blocks in SimMechanics. Contact positions and forces are measured in SimMechanics by body and joint sensors. Sampling rate for the simulations was 0.01 s.

For the simulations, the object's mass is 3 kg ($m_1 + m_2 + m_3 = 3$ kg, where m_1, m_2, and m_3 are the weights of virtual links), and its COM is located at point G as shown in Fig. 6. However, the coordinates of point G are unknown for the control system and must be estimated via kinematic adaptation law. The mass of the object is assumed to be known for the control system, assumption of a known mass for the object is not far from reality, since three force sensors at the contact points

https://doi.org/10.1017/S0263574714002379 Published online by Cambridge University Press

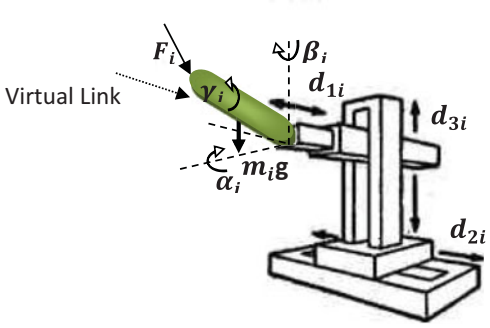


Fig. 5. Schematic of the considered robots.

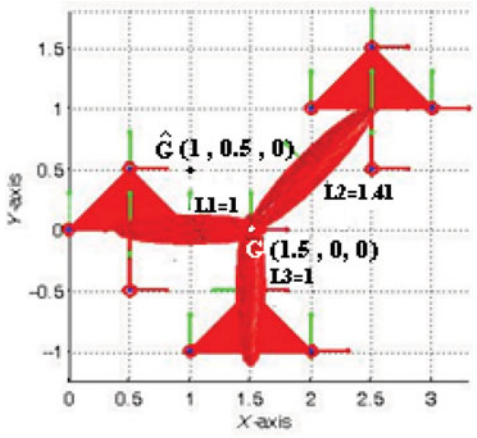


Fig. 6. An object with unknown geometry that is modeled as three virtual links.

measure the force applied to the static object at the beginning. Given the kinematics of robots, the sum of force components in the z-direction when the object is static represents the mass of the object. In the following two sections, two sets of simulation results are provided for planar and spatial desired trajectories and for two different initial positions for COM.

6.1. Simulation for planar desired trajectory

In this simulation, the desired trajectory of COM, $\boldsymbol{X}_L^d$, and its derivative, $\boldsymbol{dX}_L^d$, are defined as:

$$\boldsymbol{X}_L^d = [1.5 + \sin(0.5\pi t)\ 1 - \cos(0.5\pi t)\ 0 - 0.57\ 0.57\ 0]^{\mathrm{T}},$$
$$\boldsymbol{dX}_L^d = [0.5\pi \times \cos(0.5\pi t)\ 0.5\pi \times \sin(0.5\pi t)\ 0\ 0\ 0\ 0]^{\mathrm{T}}$$

.

The gains of shaped and locked controllers given in (27) and (51) are selected as: $\mathbf{K}_{\mathbf{p}}^{\mathbf{E}} = 125\mathbf{I}_1$, $\mathbf{K}_{\mathbf{v}}^{\mathbf{E}} = 50\mathbf{I}_1$, $\mathbf{K}_{\mathbf{p}}^{\mathbf{L}} = 450\mathbf{I}_2$, and $\mathbf{K}_{\mathbf{v}}^{\mathbf{L}} = 7500\mathbf{I}_2$, where $\mathbf{I}_1 \in \mathbf{R}^{12\times12}$ and $\mathbf{I}_2 \in \mathbf{R}^{6\times6}$.

The kinematic adaptation parameters, i.e. $\boldsymbol{\Gamma}_i$ and $\boldsymbol{\rho}_i$, are considered as:

$$\boldsymbol{\Gamma}_i = \begin{bmatrix} 1000 & 0 & 0 \\ 0 & 1000 & 0 \\ 0 & 0 & 1000 \end{bmatrix}, \text{ and } \boldsymbol{\rho}_i = \begin{bmatrix} 5 & 0 & 0 \\ 0 & 5 & 0 \\ 0 & 0 & 5 \end{bmatrix}.$$

The initial estimate for COM is given by $\hat{\boldsymbol{G}} = [1\ 0.5\ 0]^{\mathrm{T}}$.

Figure 7 shows the circular trajectory tracking of *locked* system when the COM is unknown. As shown in Figs. 8 and 9, the trajectory tracking error and orientation error of locked system rapidly

https://doi.org/10.1017/S0263574714002379 Published online by Cambridge University Press

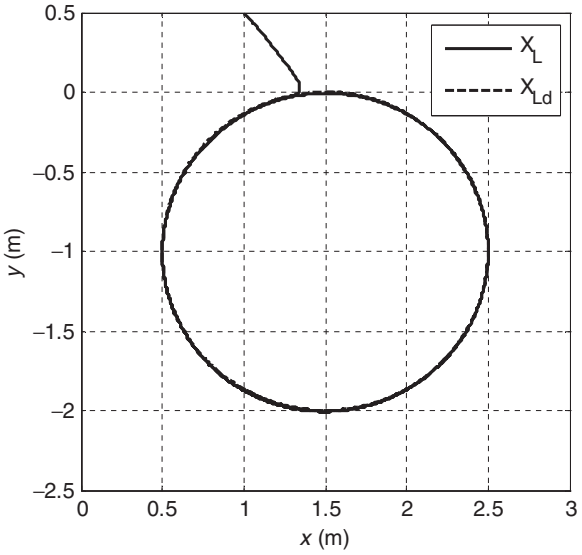


Fig. 7. Circular trajectory tracking of the locked system (the location of the estimated COM) in xy plane for $\hat{\boldsymbol{G}} = [10.50]^{\mathrm{T}}$.

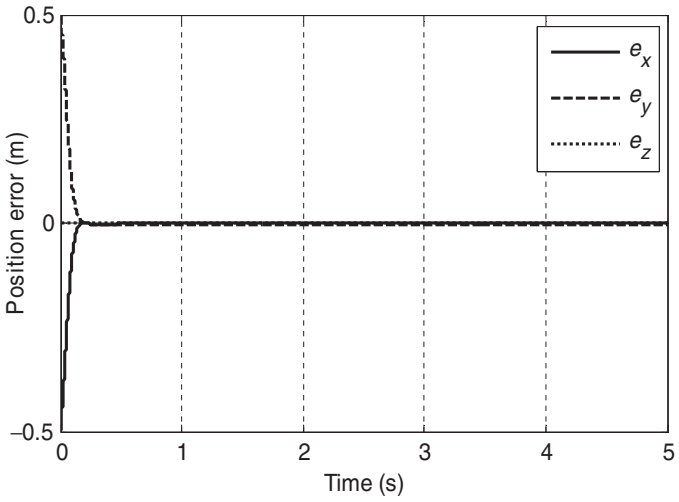


Fig. 8. Trajectory tracking error of the locked system (the location of the estimated COM) for $\hat{\boldsymbol{G}} = [10.50]^{\mathrm{T}}$.

converges to zero. Figures 10 through 14 show the convergence of kinematic and dynamic adaptation parameters. As shown in Fig. 10, the kinematic adaptation parameters converge to their real values, i.e. $L_1 = 1,\ L_2 = 1.41$, and $L_3 = 1$, as shown in Fig. 6. The dynamic parameters are also bounded, as shown in Figs. 11 through 14. The persistent excitation is necessary for the convergence of dynamic parameters to actual values. Figures 15 through 20 illustrate that the control signals are non-chattering and remain bounded, and are at an acceptable level. The initial error in Figs. 8 and 9 is due to the error in the estimation of COM. The position of COM is controlled by the locked system controller. Hence, when the position of COM is not known, the estimation of COM should be used as a reference point. As shown in Fig. 10 and by considering Fig. 6, the estimated lengths for virtual links converge to actual values, and hence the estimated COM converges to the actual COM. As shown in Fig. 10, the initial error is eliminated in less than half a second.

https://doi.org/10.1017/S0263574714002379 Published online by Cambridge University Press

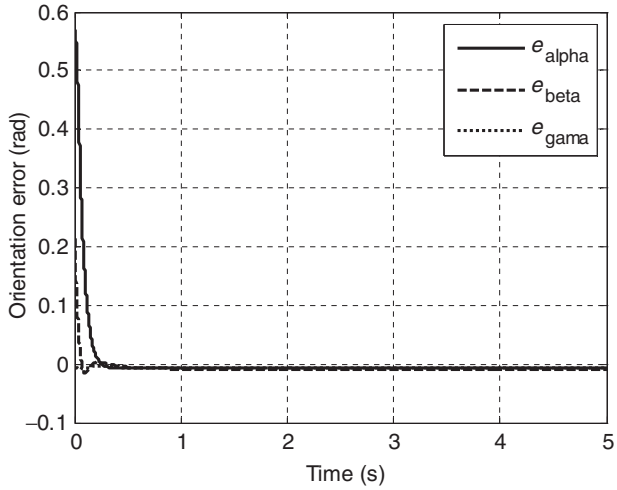


Fig. 9. Orientation error of the locked system for $\hat{\boldsymbol{G}} = [10.50]^{\mathrm{T}}$.

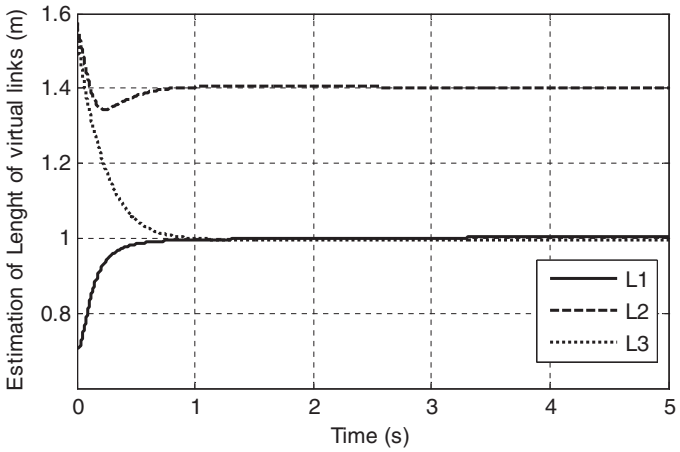


Fig. 10. Parameter convergence of the kinematic adaptive law (lengths of virtual links) for $\hat{\boldsymbol{G}} = [10.50]^{\mathrm{T}}$.

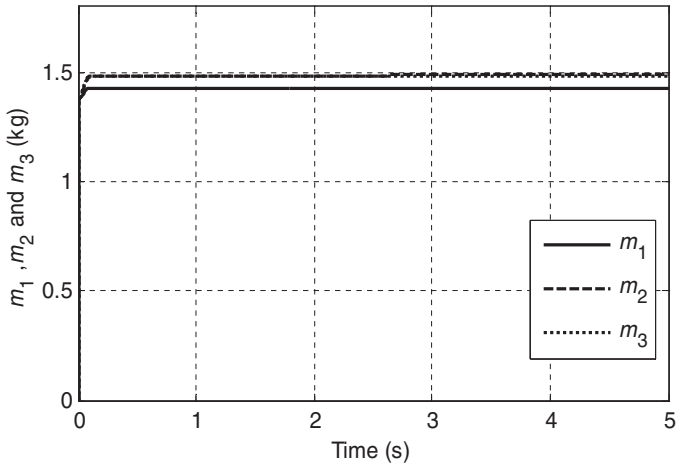


Fig. 11. Parameter convergence of the adaptation law parameters (virtual links' mass) for $\hat{\boldsymbol{G}} = [10.50]^{\mathrm{T}}$.

https://doi.org/10.1017/S0263574714002379 Published online by Cambridge University Press

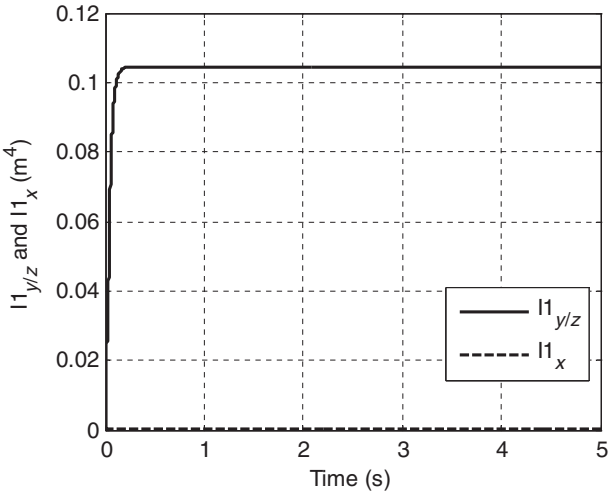


Fig. 12. Parameter convergence for the adaptation law, i.e. the virtual link's inertia associated with the first robot for $\hat{\boldsymbol{G}} = [10.50]^{\mathrm{T}}$.

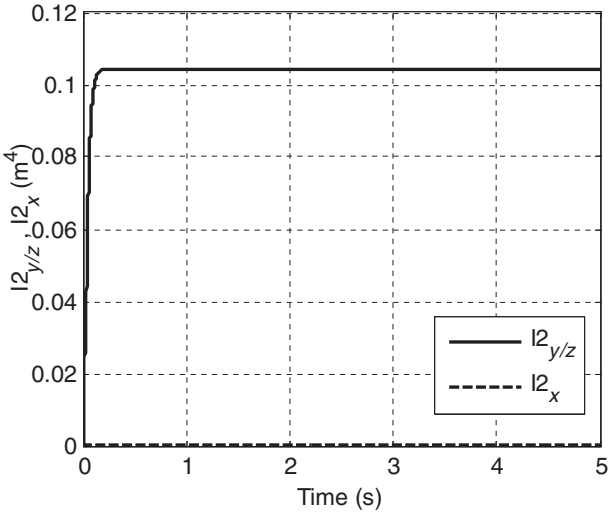


Fig. 13. Parameter convergence for the adaptation law, i.e. the virtual link's inertia associated with the second robot for $\hat{\boldsymbol{G}} = [10.50]^{\mathrm{T}}$.

6.2. Simulation for spatial desired trajectory

The following simulation results are obtained by assuming $\hat{\boldsymbol{G}} = [10.50.5]^{\mathrm{T}}$ as the initial estimate of COM, where the spatial desired trajectory is considered as follows:

$$\boldsymbol{X}_{\boldsymbol{L}}^{\boldsymbol{d}} = [-\sin(\mathrm{t})\cos(\mathrm{t}) - 1\cos(\mathrm{t}) - 0.50.50]^{\mathrm{T}},$$
$$\boldsymbol{dX}_{\boldsymbol{L}}^{\boldsymbol{d}} = [-\cos(\mathrm{t}) - \sin(\mathrm{t}) - \sin(\mathrm{t})\,000]^{\mathrm{T}}$$

.

Figures 21–23 show the trajectory tracking of object due to desired trajectory on *xy*, *xz*, and *yz* planes respectively. Figures 24 and 25 depict the position and orientation errors of *locked* system. Figure 26 illustrates the parameter convergence of the kinematic adaptive law (i.e. the lengths of virtual links).

Simulation results show that for spatial trajectory and for different initial estimations for COM, the proposed control system performs well with the locked system, and parameters of kinematic

https://doi.org/10.1017/S0263574714002379 Published online by Cambridge University Press

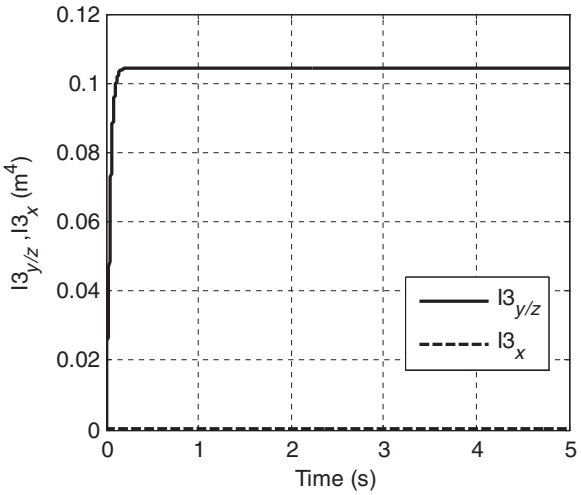


Fig. 14. Parameter convergence for the adaptation law, i.e. the virtual link's inertia associated with the third robot for $\hat{\boldsymbol{G}} = [10.50]^{\mathrm{T}}$.

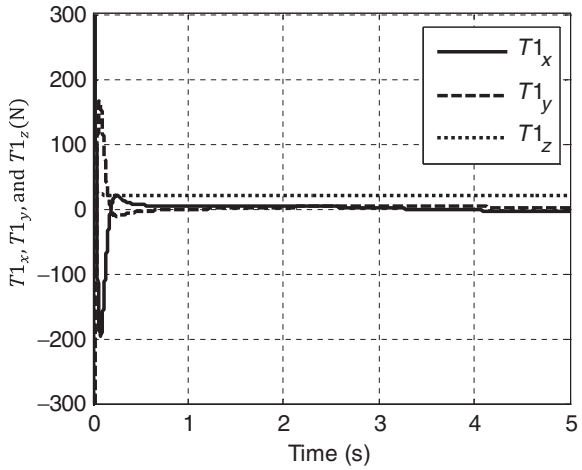


Fig. 15. Three control signals for the first robot's joints ($T1_x$, $T1_y$, and $T1_z$) for $\hat{\boldsymbol{G}} = [10.50]^{\mathrm{T}}$.

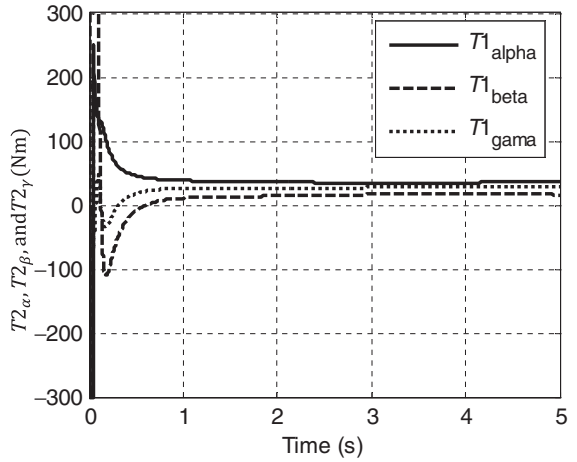


Fig. 16. Three control signals for the first robot's joints ($T1_\alpha$, $T1_\beta$, and $T1_\gamma$) for $\hat{\boldsymbol{G}} = [10.50]^{\mathrm{T}}$.

https://doi.org/10.1017/S0263574714002379 Published online by Cambridge University Press

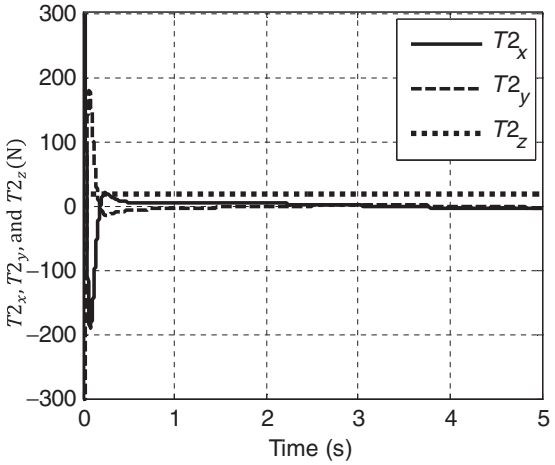


Fig. 17. Three control signals for the second robot's joints ($T2_x$, $T2_y$, and $T2_z$) for $\hat{\boldsymbol{G}} = [10.50]^{\mathrm{T}}$.

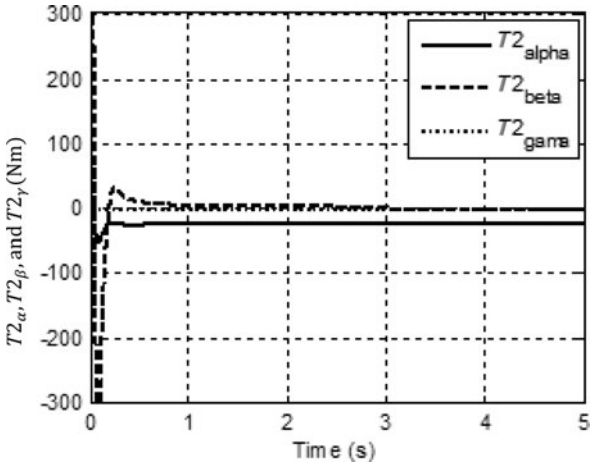


Fig. 18. Three control signals for the second robot's joints ($T2_\alpha$, $T2_\beta$, and $T2_\gamma$) for $\hat{\boldsymbol{G}} = [10.50]^{\mathrm{T}}$.

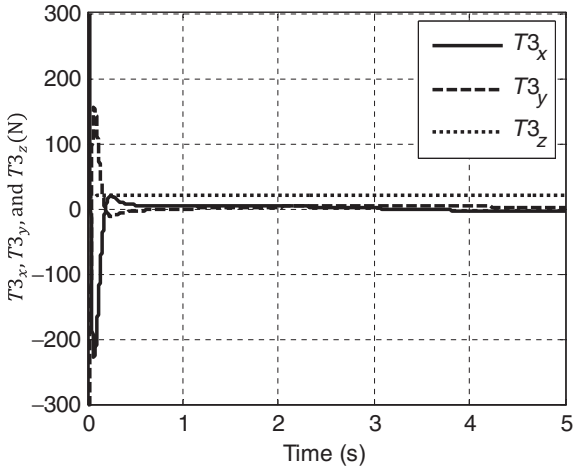


Fig. 19. Three control signals for the third robot's joints ($T3_x$, $T3_y$, and $T3_z$) for $\hat{\boldsymbol{G}} = [10.50]^{\mathrm{T}}$.

https://doi.org/10.1017/S0263574714002379 Published online by Cambridge University Press

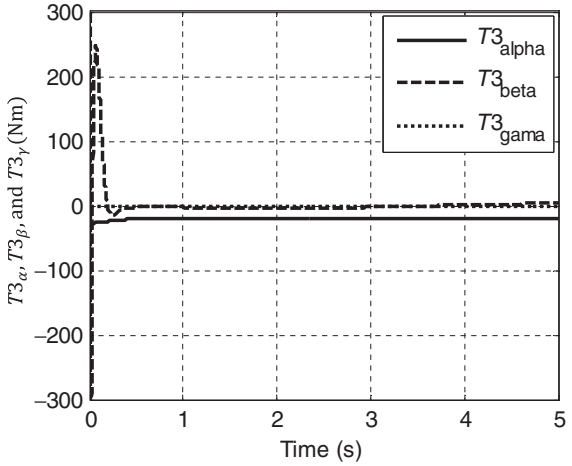


Fig. 20. Three control signals for the third robot's joints ($T3_\alpha$, $T3_\beta$, and $T3_\gamma$) for $\hat{\boldsymbol{G}} = [10.50]^{\mathrm{T}}$.

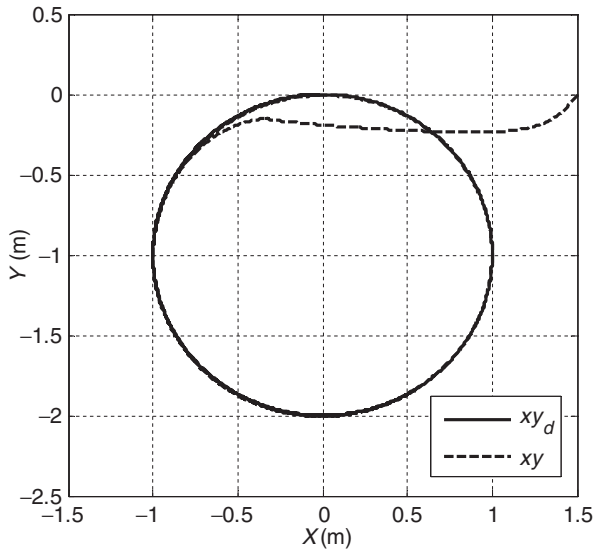


Fig. 21. Circular trajectory tracking of the locked system (location of the estimated COM) in xy plane for the second simulation for $\hat{\boldsymbol{G}} = [10.50.5]^{\mathrm{T}}$.

adaptation law converge relatively fast. Comparing the results of ref [19] with the results obtained in the current paper, the convergences of the position and orientation tracking error as well as kinematic parameters using our novel observer-based adaptive controller are much faster than the PID controller. Comparing the results of ref [20] with the current study illustrates that using a model-based controller in the current paper has increased the convergence rate significantly.

There are some issues that should be considered for implementing the proposed control system in a real robotic system. Three 3-DOF force sensors are required to measure the force at contact points continuously, which could be costly. Moreover, the rigid contact at contact points between robots and object is hard to achieve and is not the best assumption for the handling of unknown objects in real application. However, considering non-rigid contact would add redundancy to the dynamic equations of the system, which is not in the scope of the current study.

https://doi.org/10.1017/S0263574714002379 Published online by Cambridge University Press

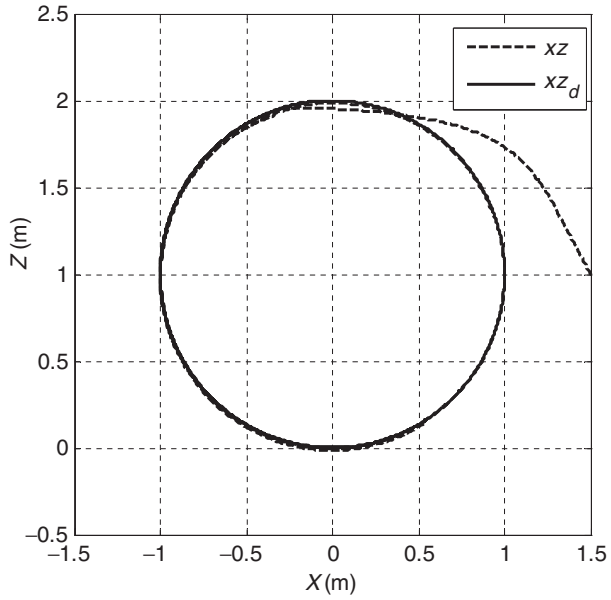


Fig. 22. Circular trajectory tracking of the locked system (location of the estimated COM) in xz plane for the second simulation for $\hat{\boldsymbol{G}} = [10.50.5]^{\mathrm{T}}$.

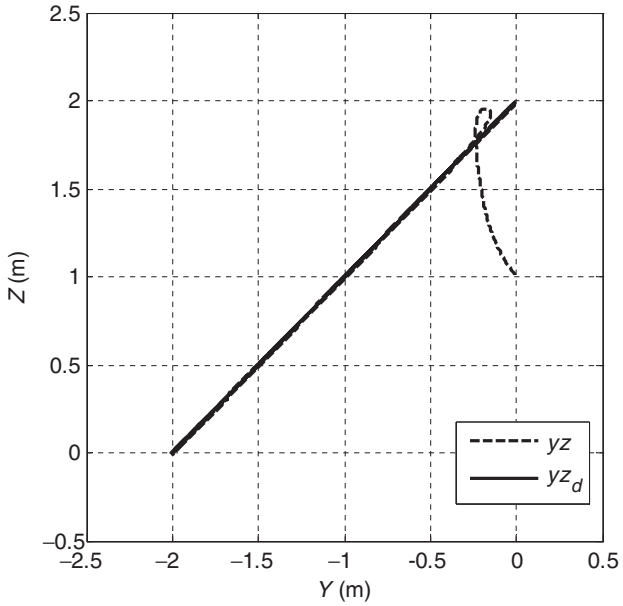


Fig. 23. Circular trajectory tracking of the locked system (location of the estimated COM) in yz plane for the second simulation for $\hat{\boldsymbol{G}} = [10.50.5]^{\mathrm{T}}$.

7. Conclusions

A cooperative robotic control system was developed for handling an object with unknown geometry, COM, and inertia using three 6-DOF robots. It was assumed that the object's mass was known and was measured using three force sensors at contact points. The geometrically unknown object was modeled by three virtual links, each of which was considered as a part of its corresponding robot. Lengths of virtual links were estimated by the kinematics adaptation law. The system dynamic equations were passively decomposed into two separate dynamics, i.e. shaped and locked dynamics. Two modified PD and observer-based adaptive controllers were developed for shaped and locked systems respectively. Dynamic parameters were also estimated using a proposed dynamic adaption

https://doi.org/10.1017/S0263574714002379 Published online by Cambridge University Press

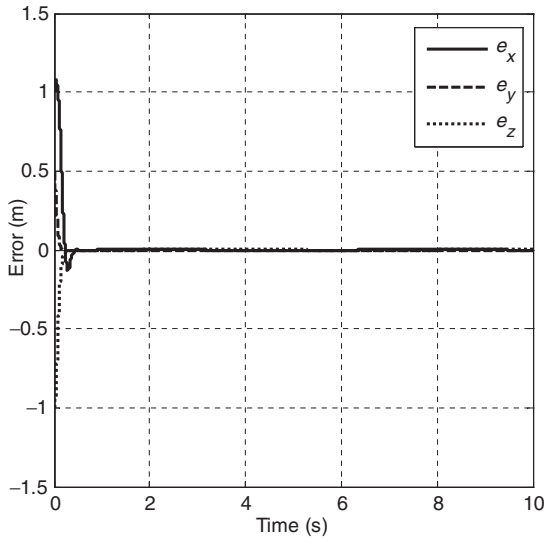


Fig. 24. Trajectory tracking error of the locked system (location of the estimated COM) for the second simulation for $\hat{\boldsymbol{G}} = [10.50.5]^{\mathrm{T}}$.

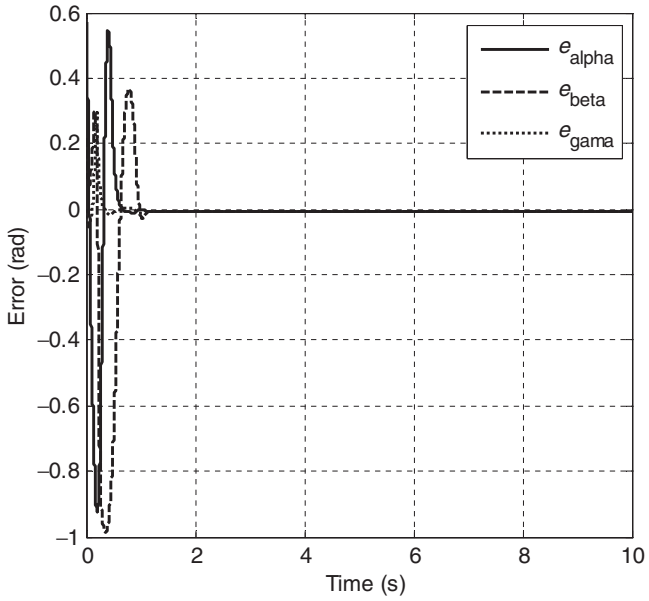


Fig. 25. Orientation error of the locked system for the second simulation for $\hat{\boldsymbol{G}} = [10.50.5]^{\mathrm{T}}$.

law. Stability of the system and convergence of coordination errors were proved by defining a Lyapunov function and using Barbalet's lemma. Simulation results show good trajectory tracking for the locked system compared with the results obtained using PID controller. The results also show bounded parameters for dynamic parameters and convergence for kinematic parameters. The results show that the proposed approach is promising for a cooperative robotic system's handling of unknown objects with kinematic and dynamic uncertainties.

Appendix A

A1. System dynamics

Using Lagrangian equations, the dynamic equation of a 6-DOF robot with a rigidly attached virtual link is given by Eqs. (A2), (A3),

https://doi.org/10.1017/S0263574714002379 Published online by Cambridge University Press

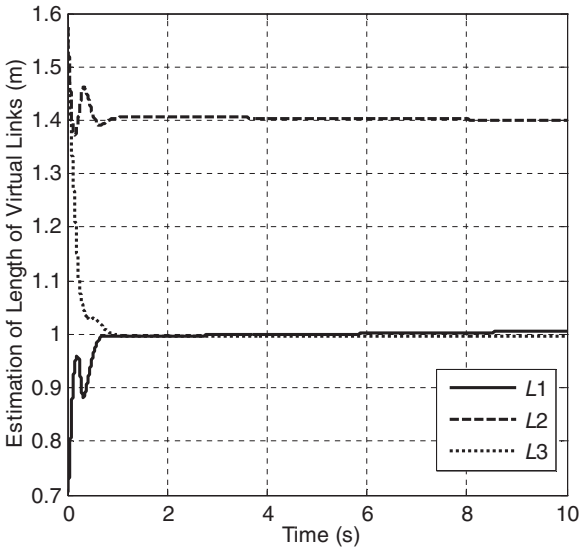


Fig. 26. Parameter convergence of the kinematic adaptive law (virtual link's length) for the second simulation for $\hat{\boldsymbol{G}} = [10.50.5]^{\mathrm{T}}$.

$$\mathbf{M_i}\left(\boldsymbol{q_i}\right) = \begin{bmatrix} m_{ix}+m_{iy}+m_{iz}+m_{il} & 0 & 0 & -l_i m_{il}\sin\alpha_i\cos\beta_i & -l_i m_{il}\cos\alpha_i\sin\beta_i & 0 \\ 0 & m_{iy}+m_{iz}+m_{il} & 0 & -l_i m_{il}\sin\alpha_i\sin\beta_i & l_i m_{il}\cos\alpha_i\cos\beta_i & 0 \\ 0 & 0 & m_{iz}+m_{il} & -l m_{il}\cos\alpha & 0 & 0 \\ -l_i m_{il}\sin\alpha_i\cos\beta_i & -l_i m_{il}\sin\alpha_i\sin\beta_i & -l_i m_{il}\cos\alpha_i & l_i^2 m_{il}+I_{il} & 0 & 0 \\ -l_i m_{il}\cos\alpha_i\sin\beta_i & l_i m_{il}\cos\alpha_i\cos\beta_i & 0 & 0 & m_{il}l_i^2\cos^2\alpha_i+I_{il} & 0 \\ 0 & 0 & 0 & 0 & 0 & I_{ix} \end{bmatrix}, \tag{A1}$$

$$\mathbf{C_i}(\boldsymbol{q_i}.\dot{\boldsymbol{q}}_{\boldsymbol{i}}) = \begin{bmatrix} 0 & 0 & 0 & -l_i m_{il}\cos\alpha_i\cos\beta_i\dot{\alpha}_i + l_i m_{il}\sin\alpha_i\sin\beta_i\dot{\beta}_i & -l_i m_{il}\cos\alpha_i\cos\beta_i\dot{\beta}_i + l_i m_{il}\sin\alpha_i\sin\beta_i\dot{\alpha}_i & 0 \\ 0 & 0 & 0 & -l_i m_{il}\cos\alpha_i\sin\beta_i\dot{\alpha}_i - l_i m_{il}\sin\alpha_i\cos\beta_i\dot{\beta}_i & -l_i m_{il}\cos\alpha_i\sin\beta_i\dot{\beta}_i - l_i m_{il}\sin\alpha_i\cos\beta_i\dot{\alpha}_i & 0 \\ 0 & 0 & 0 & l_i m_{il}\sin\alpha\dot{\alpha}_i & 0 & 0 \\ 0 & 0 & 0 & 0 & m_{il}l_i^2\cos\alpha_i\sin\alpha_i\dot{\beta}_i & 0 \\ 0 & 0 & 0 & -m_{il}l_i^2\cos\alpha_i\sin\alpha_i\dot{\beta}_i & 0 & 0 \\ 0 & 0 & 0 & 0 & 0 & 0 \end{bmatrix}. \tag{A2}$$

A2. Jacobian matrix for extended robot

The Jacobian matrix of a 6-DOF robot, $\mathbf{J}_i(\boldsymbol{q})$, with rigidly attached virtual link can be obtained as follows:

$$\begin{pmatrix} \dot{x}_i \\ \dot{y}_i \\ \dot{z}_i \\ \dot{\alpha}_i \\ \dot{\beta}_i \\ \dot{\gamma}_i \end{pmatrix} = \overbrace{\begin{pmatrix} 1 & 0 & 0 & -l_i\cos\beta_i\sin\alpha_i & -l_i\sin\beta_i\cos\alpha_i & 0 \\ 0 & 1 & 0 & -l_i\sin\beta_i\sin\alpha_i & l\cos\beta_i\cos\alpha_i & 0 \\ 0 & 0 & 1 & -l_i\cos\alpha_i & 0 & 0 \\ 0 & 0 & 0 & 1 & 0 & 0 \\ 0 & 0 & 0 & 0 & 1 & 0 \\ 0 & 0 & 0 & 0 & 0 & 1 \end{pmatrix}}^{\mathbf{J}_i(\boldsymbol{q})} \begin{pmatrix} \dot{d}_{1i} \\ \dot{d}_{2i} \\ \dot{d}_{3i} \\ \dot{\alpha}_i \\ \dot{\beta}_i \\ \dot{\gamma}_i \end{pmatrix}, \tag{A3}$$

where $\mathbf{l_i}$ is the length of the virtual link connected to the ith robot. $\mathrm{d_{1i}}$, $\mathrm{d_{2i}}$, and $\mathrm{d_{3i}}$ are x, y, and z axes coordinates of the ith robot shown in Fig. 5.

https://doi.org/10.1017/S0263574714002379 Published online by Cambridge University Press

Appendix B

Notations

No.	Symbol	Definition
1.	${}^{b}\boldsymbol{r}_{i}$	Vector that represents the *i*th virtual link with respect to base coordinate frame.
2.	${}^{b}\boldsymbol{r}_{ix}$	X component of ${}^{b}\boldsymbol{r}_{i}$ vector.
3.	${}^{b}\boldsymbol{r}_{iy}$	Y component of ${}^{b}\boldsymbol{r}_{i}$ vector.
4.	${}^{b}\boldsymbol{r}_{iz}$	Z component of ${}^{b}\boldsymbol{r}_{i}$ vector.
5.	L_i	Length of the *i*th virtual link corresponding to *i*th robot.
6.	m_i	Mass of the *i*th virtual link corresponding to *i*th robot.
7.	I_{xi}	Inertia of the *i*th virtual link with respect to *x*-axis, where *x* is defined along the virtual link.
8.	$I_{y/zi}$	Inertia of the *i*th virtual link with respect to *y*- and *z*-axis.
9.	$\sum$	Base frame.
10.	$\sum_{\mathrm{b}}$	Object frame that has the same orientation as the base frame.
11.	$\sum_{\mathrm{o}}$ $\sum_{\mathrm{o}'}$	Frame attached to the object's center of mass, which rotates with the object.
12.	$\boldsymbol{q}_i$	The generalized coordinate vector of each robot.
13.	$\mathbf{M_i}(\boldsymbol{q}_i)$	Inertia matrix of the *i*th robot.
14.	$\mathbf{C_i}(\boldsymbol{q}_i, \dot{\mathbf{q}}_\mathbf{i})$	Coriolis matrix of the *i*th robot.
15.	$\boldsymbol{\tau}_i$	Control generalized force to be designed in joint space.
16.	$\boldsymbol{F}_i$	External force in task space corresponding to *i*th extended robot.
17.	$\mathbf{J_i}(\boldsymbol{q})$	The Jacobian matrix to transform from joint space into task space for *i*th extended robot.
18.	$\boldsymbol{\theta}_{\mathbf{id}}$	Dynamic parameter vector for the *i*th extended robot.
19.	$\boldsymbol{p}_{v,i}$	Position of the tip of virtual links with respect to base coordinate system.
20.	$\boldsymbol{\phi}_{v,i}$	Orientation of the *i*th virtual link end effecter in terms of Euler angles.
21.	$\mathbf{Y_i}$	Dynamic regressor matrix of the *i*th extended robot.
22.	$\boldsymbol{X}$	Cooperative robotic system coordinates.
23.	$\boldsymbol{X}_i$	*i*th extended robot coordinates in task space.
24.	x_i	X component of position vector of virtual link's end effecter corresponding to the *i*th robot in task space.
25.	y_i	Y component of position vector of virtual link's end effecter corresponding to the *i*th robot in task space.
26.	z_i	Z component of position vector of virtual link's end effecter corresponding to the *i*th robot in task space.
27.	α_i	Rotational of virtual link's end effecter corresponding to the *i*th robot with respect to *z*-axis.
28.	β_i	Rotational of virtual link's end effecter corresponding to the *i*th robot with respect to *y*-axis.
29.	γ_i	Rotational of virtual link's end effecter corresponding to the *i*th robot with respect to *x*-axis.
30.	$\boldsymbol{X}_E$	Shaped system coordinates.
31.	$\boldsymbol{X}_L$	Locked system coordinates.
32.	$\boldsymbol{P}_L$	Translational components vector of locked system coordinate.
33.	$\boldsymbol{\phi}_L$	Rotational components vector of locked system coordinate.
34.	$\mathbf{S}$	Decomposition matrix.
35.	$\mathbf{T}$	Transformation matrix from joint space to object space.
36.	$\boldsymbol{\rho}$	Positive definite matrix for damping term of kinematic adaptation law.
37.	$\boldsymbol{F}_i$	External force in task space.
38.	$\boldsymbol{F}_{ci}(k)$	Contact force corresponding to the *i*th robot.
39.	$\mathbf{M_i}(\boldsymbol{X}_i)$	Inertia matrix of the *i*th robot in task space.
40.	$\mathbf{M_L}(\boldsymbol{X})$	Inertia matrix of the locked system.

https://doi.org/10.1017/S0263574714002379 Published online by Cambridge University Press

41. $\mathbf{M_E}(\boldsymbol{X})$ Inertia matrix of the shaped system.
42. $\mathbf{C_E}$ Coriolis matrix for the shaped system in object space.
43. $\mathbf{C_L}$ Coriolis matrix for the shaped system in object space.
44. $\mathbf{C_{EL}}$ Coupling term for the shaped system.
45. $\mathbf{C_{LE}}$ Coupling term for the locked system.
46. $\boldsymbol{F_E}$ External force for the shaped system in object space.
47. $\boldsymbol{F_L}$ External force for the locked system in object space.
48. $\hat{\boldsymbol{F}}_{\boldsymbol{L}}$ Estimation of external force for the locked system.
49. $\boldsymbol{T_E}$ Control signals for shaped system.
50. $\boldsymbol{T_L}$ Control signals for locked system.
51. $\boldsymbol{X}_{\boldsymbol{E}}^{\boldsymbol{d}}$ Desired shaped coordinate.
52. $\hat{\beta}_i$ Estimated value for β_i.
53. $\boldsymbol{X}_{ci}$ Position vector of contact point corresponding to *i*th robot.
54. $\hat{\boldsymbol{X}}_{ci}$ Estimation of contact point.
55. $\boldsymbol{X_o}$ Position vector of object's COM.
56. $\hat{\boldsymbol{X}}_{\boldsymbol{o}}$ Object's estimated COM.
57. Γ_i Positive definite constant matrix of kinematic adaptation law.
58. $\boldsymbol{\rho}_i$ Positive definite constant matrix for damping term of kinematic adaptation law.
59. $\boldsymbol{e}_i$ Error between the measured coordinates of the contact point and the estimated one corresponding to the *i*th robot.
60. $\boldsymbol{T_c}$ Decoupling controller.
61. $\boldsymbol{T_E}$ Control actions for shaped system.
62. $\mathbf{T_L}$ Control actions for locked system.
63. $\mathbf{K_p^E}$ P-gain matrix for the shaped system PD controller.
64. $\mathbf{K_d^E}$ D-gain matrix for the shaped system PD controller.
65. $\mathbf{K}'$ Positive definite matrix for the damping term of the shaped system controller.
66. $\mathbf{K_p^L}$ P-gain matrix for PID controller of the locked system.
67. $\dot{\boldsymbol{q}}_{ir}$ *i*th robot's reference velocity in the joint space.
68. $\dot{\boldsymbol{X}}_{\boldsymbol{Er}}$ Reference velocity of the shaped system.
69. $\dot{\boldsymbol{X}}_{\boldsymbol{Lr}}$ Reference velocity of the locked system.
70. $\dot{\boldsymbol{X}}_{\boldsymbol{Ld}}$ Desired velocity vector for the locked system.
71. $\ddot{\boldsymbol{X}}_{\boldsymbol{Ld}}$ Desired acceleration vector for the locked system.
72. $\boldsymbol{e_E}$ Closed-loop error vectors for the shaped system.
73. $\boldsymbol{e_L}$ Closed-loop error vectors for the locked system.
74. $\boldsymbol{\lambda_i}$ Positive definite constant matrices for sliding vector.
75. $\boldsymbol{\theta}_{\boldsymbol{od}}$ Dynamic parameter vector for the entire system.
76. $\boldsymbol{\theta}_{\boldsymbol{Ed}}$ Dynamic parameter vector for the shaped system.
77. $\boldsymbol{\theta}_{\boldsymbol{Ld}}$ Dynamic parameter vector for the locked system.
78. $\boldsymbol{Y}_{\boldsymbol{or}}$ Regressor matrix of the entire system.
79. $\boldsymbol{Y}_{\boldsymbol{Er}}$ Regressor matrix of the shaped system.
80. $\boldsymbol{Y}_{\boldsymbol{Lr}}$ Regressor matrix of the locked system.
81. $\boldsymbol{s_L}$ Sliding vector for locked system.
82. $\hat{\boldsymbol{s}}_{\boldsymbol{L}}$ Estimation of sliding vector for locked system.
83. $\mathbf{k}$ Positice definite constant matrices for locked system controller.
84. $\mathbf{k_d}$ Positice definite constant matrices for the proportianl gain of the locked system controller.
85. $\tilde{\boldsymbol{\theta}}_{\boldsymbol{Ld}}$ Dynamic parameters' vector estimation error for the locked system.
86. $\tilde{\boldsymbol{F}}_{\boldsymbol{L}}$ External force estimation error for the locked system.
87. $\mathbf{P}$ Positive definite constant matrix.
88. $\mathbf{\Gamma_L}$ Positive definite constant matrix.
89. V_E Lyapunov function for the shaped system.
90. V_L Lyapunov function for the locked system.

https://doi.org/10.1017/S0263574714002379 Published online by Cambridge University Press

References

1. J. J. Craig, P. Hsu and S. S. Sastry, "Adaptive control of mechanical manipulators," *Int. J. Robot. Res.* **6**(2), 16–28 (1987).
2. P. Hsu, M. Bodson, S. Sastry and B. Paden, "Adaptive identification and control for manipulators without using joint accelerations," *Proceedings of the International Conference on Robotics and Automation*, vol. 4, Raleigh, NC, USA (Mar. 31–Apr. 3, 1987) pp. 1210–1215.
3. J. J. E. Slotine and W. Li, "On the adaptive control of robot manipulators," *Int. J. Robot. Res.* **6**(3), 49–59 (1987).
4. C. C. Cheah, M. Hirano, S. Kawamura and S. Arimoto, "Approximate Jacobian control for robots with uncertain kinematics and dynamics," *IEEE Trans. Robot. Autom.* **19**(4), 692–702 (2003).
5. C. C. Cheah, S. Kawamura and S. Arimoto, "Feedback control for robotic manipulators with an uncertain Jacobian matrix," *J. Robot. Syst.* **12**(2), 119–134 (1999).
6. C. C. Cheah, C. Liu and J. J. E. Slotine, "Approximate Jacobian Adaptive Control for Robot Manipulators," *Proceedings of the 2004 IEEE International Conference on Robotics and Automation*, vol. 3, New Orleans, LA, USA (Apr. 26–May 1, 2004) pp. 3075–3080.
7. C. C. Cheah, C. Liu and J. J. E. Slotine, "Adaptive Jacobian Tracking Control of Robots Based on Visual Task-Space Information," *Proceedings of the 2005 IEEE International Conference on Robotics and Automation*, Barcelona, Spain (Apr. 18–22, 2005) pp. 3498–3503.
8. J. Gudiño-Lau and M. A. Arteaga, "Dynamic model and simulation of cooperative robots: A case study," *Int. J. Robot.* **23**(5), 615–624 (2005).
9. J. Gudiño-Lau, M. A. Arteaga, L. A. Muñoz and V. Parra-Vega, "On the control of cooperative robots without velocity measurements," *IEEE Trans. Control Syst. Technol.* **12**(4), 600–608 (2004).
10. T. Tsuji, A. Jazidie and M. Kaneko, "Distributed trajectory generation for cooperative multi-arm robots via virtual force interactions," *IEEE Trans. Syst. Man Cybern. B* **27**(5), 862–867 (1997).
11. D. Lee and M. W. Spong, "Bilateral Teleoperation of Multiple Cooperative Robots over Delayed Communication Networks: Theory," *Proceedings of the International Conference on Robotics and Automation*, Barcelona, Spain (Apr. 18–22, 2005) pp. 360–365.
12. D. Lee, O. M. Palafox and M. W. Spong, "Bilateral Teleoperation of Multiple Cooperative Robots over Delayed Communication Networks: Application," *Proceedings of the International Conference on Robotics and Automation*, Barcelona, Spain (Apr. 18–22, 2005) pp. 366–371.
13. S. Sirouspour, "Robust Control Design for Cooperative Teleoperation," *Proceedings of the International Conference on Robotics and Automation*, Barcelona, Spain (Apr. 18–22, 2005) pp. 1133–1138.
14. H. Kawasaki, S. Ueki and S. Ito, "Decentralized adaptive coordinated control of multiple robot arms without using a force sensor," *Int. J. Autom.* **42**(3), 481–488 (2006).
15. C. P. Tang and V. N. Krovi, "Manipulability-based configuration evaluation of cooperative payload transport by mobile manipulator collectives," *Int. J. Robot.* **25**(1), 29–42 (2007).
16. H. Sarikaya, R. Burkan and I. Uzmay, "Robust and adaptive control of three dimensional revolute-jointed cooperative manipulators for handling automation," *Int. J. Robot.* **24**(2), 163–172 (2006).
17. R. Rastegari and S. A. A. Moosavian, "Multiple Impedance Control of Cooperative Manipulators Using Virtual Object Grasp," *Proceedings of the IEEE International Conference on Control Applications*, Munich, Germany (Oct. 4–6, 2006) pp. 2872–2877.
18. R.Tinós, M. Henrique Terra and J. Y. Ishihara, "Motion and force control of cooperative robotic manipulators with passive joints," *IEEE Trans. Control Syst. Technol.* **14**(4), 725–734 (2006).
19. R. Monfaredi, S.M. Rezaei and H.A. Talebi, "A cooperative robotic system for handling a geometrically unknown object," *Int. J. Control Syst. IMechE I.* **224**(8), 970–982 (2010).
20. R. Monfaredi, S. M. Rezaei and H. A. Talebi, "A Cooperative Robotic System for Handling a Geometrically Unknown Object for Non-rigid Contact Without Force Sensors," *Proceedings of the IEEE International Conference on Robotics and Biomimetics (ROBIO)*, Phuket, Thailand (Dec. 7–11, 2011) pp. 240–245.
21. R. Mohajerpoor, S. M. Rezaei, H. A. Talebi and R. Monfaredi, "A Robust Adaptive Control Scheme for Two Planar Manipulators Handling an Unknown Object in an Assembly Process," *Proceedings of the IEEE International Conference on Robotics and Biomimetics (ROBIO)*, Phuket, Thailand (Dec. 7–11, 2011) pp. 156–161.
22. R. Mohajerpoor, S. M. Rezaei, H. A. Talebi and R. Monfaredi, "An Adaptive Hybrid Control Scheme for Two Planar Manipulators Handling an Unknown Object in an Assembly Process," *Proceedings of the 2nd International Conference on Control, Instrumentation and Automation (ICCIA)*, Shiraz, Iran (Dec. 2011) pp. 835–840.
23. R. Mohajerpoor, M. Rezaei, H. A. Talebi, M. Noorhosseini and R. Monfaredi, "A robust adaptive hybrid force/position control scheme of two planar manipulators handling an unknown object interacting with an environment," Proceedings of the Institution of Mechanical Engineers, part I, *J. Syst. Control Eng.*, **226**(4), 509–522 (2012).
24. R. Seifabadi, S. M. Rezaei, S. S. Ghidary, M. Zareinejad and M. Saadat, "To enhance transparency of a Piezo-actuated tele-micromanipulator using passive bilateral control," *Robotica* **28**(5), 689–703 (2010) (Cambridge University Press).
25. D. Lee and P. Y. Li, "Passive bilateral control and tool dynamics rendering for nonlinear mechanical teleoperator," *IEEE Trans. Robot.* **21**(5), 936–951 (2005).

https://doi.org/10.1017/S0263574714002379 Published online by Cambridge University Press